MEASUREMENT OF NEUTRON FLUENCE SPECTRA USING A PASSIVE NESTED NEUTRON SPECTROMETER WITH GOLD FOILS

Felix Mathew

Medical Physics Unit

McGill University, Montreal

August 2019

A thesis submitted to McGill University in partial fulfillment of the requirement of the degree of Master of Science in Medical Radiation Physics.

Acknowledgements

First and foremost, I thank god for giving me the knowledge, strength and ability to complete this work.

I am grateful to my supervisor John Kildea who gave me the opportunity to work with him, and supported me throughout this project. It is impossible to verbalize my gratitude for everything he did for me, as my teacher and supervisor. I also thank my program director Jan Seuntjens who helped me directly and indirectly in many ways in my student life as well as the time I spent with the Medical Physics Unit.

There were so many wonderful people involved in this project, and I am lucky to have their support and encouragement. I would like to thank the director of the SLOWPOKE Neutron Activation Analysis Laboratory, Polytechnique Montreal, Cornelia Chilian for helping and guiding me with the activation analysis. Thank you for being very kind to me. I am grateful to my friend and colleague, Logan Montgomery for all the guidance and support he provided; from showing me how to operate a Linac to completing this written work. I acknowledge his sincere help and contribution in every step involved. I thank our radiation safety officer Michael Evans for being equally excited as me to do the gold activation study, and supporting me. I thank all my colleagues and friends, especially Chris and Santiago for being there with me through the hard times. They helped me physically and mentally in the time of needs and I am very grateful. I would like to express my thanks to our NNS vendor Jacques Dubeau who provided his knowledge and expertise

in neutron spectrometry.

This wouldn't have been possible without my family and their encouragement. I thank my father, mother, sister and brother for all the love and support.

Thank you all.

"When you arrive at the destination, never forget where the journey began." — Lailah Gifty Akita

"Saying thank you is more than good manners. It is good spirituality." — Alfred Agache

Abstract

During high-energy radiotherapy, secondary neutrons are generated as an unwanted byproduct. It is imperative to accurately determine the neutron spectrum in order to assess the secondary cancer risks posed to the patients by these neutrons. Instruments like the Nested Neutron Spectrometer (NNS) can be used to measure the neutron fluence spectra but the active neutron detector in the spectrometer may be inaccurate when the neutron fluence rate is high due to pulse pileup. We developed a passive NNS with gold foils that may be operated in high fluence rate environments without suffering from pulse pileup.

The passive NNS was used to measure the neutron fluence spectrum at 100 cm from isocentre, along the treatment couch, that was generated by a Varian TrueBeam linac operated at 15 MV. The specific saturation activities of the irradiated gold foils were determined post-irradiation using a high purity germanium detector.

To process the measured activities, the response functions of the passive NNS were required. The response functions were generated by first modelling the passive NNS, including moderator shells and gold foils, within the Geant4 v10.4 simulation environment. Simulated irradiations of monoenergetic neutrons were then performed to determine the number of (n,γ) neutron capture reactions per unit neutron fluence as a function of neutron energy (i.e. detector response). The response functions generated showed that the detector response shifts to higher energies as the neutron moderator thickness increases, as expected.

Using the response functions, the data were iteratively unfolded (i.e. deconvoluted) using the Maximum-Likelihood Expectation-Maximization (MLEM) algorithm to obtain the neutron fluence-rate spectrum at the location of the measurement. The spectrum had two prominent peaks: (i) a dominant peak at the fast neutron energy and (ii) a small peak at the thermal energies. This spectrum was also compared with the spectrum generated with a conventional NNS.

Résumé

Au cours de la radiothérapie à haute énergie, les neutrons secondaires sont générés en tant que sous-produit indésirable. Il est impératif de déterminer avec précision le spectre des neutrons afin d'évaluer les risques de cancer secondaires que ces neutrons présentent pour les patients. Des instruments tels que le Nested Neutron Spectrometer (NNS) peuvent être utilisés pour mesurer les spectres de la fluence neutronique, mais le détecteur de neutrons actifs dans le spectromètre peut être imprécis lorsque le taux de fluence neutronique est élevé en raison de la superposition d'impulsions. Nous avons développé un NNS passif avec des feuilles d'or pouvant être utilisé dans des environnements à taux de fluence élevé sans souffrir d'empilement.

Le NNS passif a été utilisé pour mesurer le spectre de la fluence neutronique à 100 cm de l'isocentre, le long du lit de traitement, généré par un linac Varian TrueBeam fonctionnant à 15 MV. Les activités de saturation spécifiques des feuilles d'or irradiées ont été déterminées après irradiation à l'aide d'un détecteur au germanium de haute pureté.

Pour traiter les activités mesurées, les fonctions de réponse du système NNS passif étaient nécessaires. Les fonctions de réponse ont été générées en modélisant d'abord le système NNS passif, y compris les coques de modérateur et les feuilles d'or, dans l'environnement de simulation Geant4 v10.4. Des irradiations simulées de neutrons monoénergétiques ont ensuite été effectuées pour déterminer le nombre de réactions de capture de neutrons (n, γ) par unité de fluence neutronique en fonction de l'énergie des neutrons (c'est-à-dire la réponse du détecteur). Les fonctions de réponse

générées ont montré que la réponse du détecteur passe à des énergies plus élevées à mesure que l'épaisseur du modérateur de neutrons augmente, comme prévu.

En utilisant les fonctions de réponse, les données ont été dépliées de manière itérative (c'est-à-dire déconvolué) avec l'algorithme MLEM (Maximum-Likelihood Expectation-Maximization) pour obtenir le spectre du taux de fluence neutronique à l'emplacement de la mesure. Le spectre présentait deux pics importants : (i) un pic dominant pour l'énergie des neutrons rapides et (ii) un petit pic pour les énergies thermiques. Ce spectre a également été comparé au spectre généré avec un NNS conventionnel.

Contribution of the author

All the chapters in this thesis were solely written by the author.

Chapter 1: Introduction and Chapter 2: Theory were written by the author after a comprehensive review of the relevant literature.

The passive Nested Neutron Spectrometer was developed by modifying the original Nested Neutron Spectrometer (NNS, Detec Inc, Gatineau, Quebec). Response functions for the passive NNS were generated by the author, who developed and executed the simulations in Geant4. Subsequently, the experimental data were obtained by the author using both the passive NNS and the conventional NNS. The activation analysis of the gold foils were performed under the guidance of Dr. Cornelia Chilian at Polytechnique Montréal, who had previously calibrated the HPGe spectrometer independent of the author. An in-house MLEM algorithm, written in C++, was modified by the author and was used to unfold the spectral measurements, resulting in the neutron fluence spectra of interest.

The results and analysis presented in Chapters 4 and 5 were prepared by the author under the guidance of their supervisor.

Contents

List of Figures

List of Tables

Chapter 1

Introduction

1.1 Cancer description

According to the publication Global Cancer Statistics [1], cancer is the primary cause of death in economically developed countries and the second leading cause of death in developing countries. The Canadian Cancer Society estimated [2] that about 50% of Canadians are expected to be diagnosed with cancer at some point in their life, and about 25% of the total population in Canada may die from cancer. It is essential to understand what cancer is in order to comprehend different means to curb the disease.

The cells in our body usually grow, perform their tasks, multiply and then ultimately die according to the instructions provided by the genes within them. But sometimes these genes fail to give accurate instructions due to mutations, which results in abnormal and uncontrolled cell growth and division. This abnormal cell growth and division that result in the formation of lumps in different parts of our body are called solid tumors, and that do not form a lump are called non-solid tumors (e.g. Leukemia). Benign tumors are non-cancerous lesions that do not spread or invade other tissues, whereas malignant (cancerous) tumors can spread to other parts of the body via the

blood or lymphatic systems.

Cancer is a genetic disease caused mainly by the mutation of particular genes: proto-oncogenes, tumor suppressor genes and DNA repair genes [3]. Mutations can be induced by environmental exposure to chemicals and radiation or can be inherited genetically.

1.2 Cancer treatment modalities

Today, there are many different cancer treatment modalities. Numerous factors such as the cancer type, cancer characteristics, staging, position, size, patient conditions and patient wishes influence the choice of the treatment [4]. Additionally, depending on the tumor/patient conditions, the treatment can either be palliative or curative. A palliative treatment is often provided as terminal care for the patient with the objective of alleviating the pain and associated symptoms of cancer [5], whereas a curative treatment is prescribed to eradicate the disease and cure the patient of it. The most common forms of cancer treatment are described in the following subsections.

1.2.1 Surgery

Surgery plays an important role in cancer care, and it is the oldest form of treatment [6]. Although surgery may be able to resect the tumour, it is not always feasible due to the complications associated with the tumor, its location, patient conditions and so on. The intent of performing a surgery can be the absolute removal of the tumor, but complete excision may not always be possible. Therefore, surgery is often followed by chemotherapy or radiation therapy to treat residual disease.

1.2.2 Chemotherapy

Chemotherapy uses cytoxic chemicals with the ability to destroy cells [7]. These drugs are often administered in combination with one or more other pharmaceuticals that specifically target tumor cells or that can reduce normal cell toxicity. Chemotherapy can be performed with the objective of eradicating the tumor completely, however it is also often used in conjunction with other modalities and is consequently denoted: neoadjuvant therapy or adjuvant therapy. In neoadjuvant chemotherapy, drugs are used to reduce the tumor volume before a main course of radiation treatment, whereas in adjuvant therapy, chemotherapy is performed after surgery or radiotherapy to destroy cancer cells that remain after the preliminary treatment.

1.2.3 Radiotherapy

Radiotherapy uses high doses of ionizing radiation consisting of high-energy photons, electrons, or other particles to destroy cancerous cells. Through ionization, the radiation damages cellular DNA via single and double strand breaks, making it impossible for the cells to divide. Radiation therapy can be delivered before, during or after other treatment procedures with the intent of reducing the cancer size or destroying the cancer cells that are left behind by the prior treatment.

There are two major modes of radiation therapy: external beam radiotherapy and brachytherapy. In external beam radiotherapy, the radiation is generated outside of the patient's body and directed towards the treatment site. In brachytherapy, the source of radiation is placed next to the tumor or inside the tumor itself. Ionizing radiation for external beam radiotherapy can be obtained from radioactive isotopes or it can be generated using charged particle accelerators like linear accelerators. Medical linear accelerators (linacs) are widely-used sources of ionizing radiation for external beam radiotherapy.

Medical linear accelerators

A linac consists of an electron gun (an electron source), an accelerating wave-guide, a high-Z target and other auxiliary components [8]. The electron gun, also known as the injection system of a linac, thermionically emits electrons from its heated cathode. These electrons travel to the wave-guide where they are accelerated to very high energies using an electromagnetic field. For the treatment of superficial tumors, the accelerated electron beam is delivered to a scattering foil and subsequently collimated to match the treatment field. When high-energy photons are required to treat a lesion at depth, the electron beams are made to hit a high-Z target wherein photons are generated via bremsstrahlung interactions. A typical linac can generate electron and photon beams at various megavoltage energies in the range of 6-22 MeV and 6-18 MV, respectively.

1.3 Neutrons in radiotherapy

1.3.1 Generation

Many beam-shaping and shielding components in the head of the linac are composed of high Z materials such as tungsten (W) and lead (Pb). When the linac is operated above approximately 8 MV, some photons have higher energy than the neutron binding energy ($\sim$7 MeV) of the relevant high Z nuclei [9] and can thus liberate neutrons through (γ,n) nuclear reactions. These neutrons are called the photo-neutrons. Similarly, when the linac is operated in high-energy electron mode, electroneutrons are generated through $(e,e'n)$ interactions [10]. However, photoneutrons are the subject of most studies regarding neutrons in radiotherapy because electroneutrons are relatively less significant due to having a production cross-section of about 137 times lower than that of photoneutrons [11].

Two photon-nucleus interactions that lead to the generation of photoneutrons are evaporation and direct photoionization. In evaporation, the energy of the photon is shared among several

interacting nucleons and one or more "evaporation" neutron(s) emerge(s) with energy(ies) around 1 MeV [9]. On the other hand, in direct photoinonization, the photon transfers all of its energy to a single neutron, denoted as a "knock-on" neutron [9].

1.3.2 Classification

Neutrons with energies $\sim$ 0.025 eV are called the thermal neutrons. According to the Maxwell-Boltzmann distribution, 0.025 eV is the most probable neutron energy under thermal equilibrium at room temperature [4]. In general, neutrons are classified on the basis of their kinetic energy E_k, with thermal neutrons as the reference. There are multiple variants of the neutron classification, but the one used in this study is the following [8]:

1. Ultracold neutrons with $E_k < 2 \times 10^{-7}$ eV
2. Very cold neutrons with $2 \times 10^{-7} eV \leq E_k \leq 5 \times 10^{-5}$ eV
3. Cold neutrons with $5 \times 10^{-5} eV \leq E_k \leq 0.025$ eV
4. Thermal neutrons with $E_k \approx 0.025$ eV
5. Epithermal neutrons with 1 eV $< E_k <$ 1 keV
6. Intermediate neutrons with 1 keV $< E_k <$ 0.1 MeV
7. Fast neutrons with $E_k > 0.1$ MeV

1.3.3 Biological risks associated with neutrons

The secondary fast neutrons generated in the head of the linac may be moderated, i.e. slowed down, due to elastic and inelastic scattering in the walls and furnishings of the treatment room. Therefore,

the neutron spectra inside a radiotherapy bunker typically consist of thermal, epithermal and fast neutrons.

Fast neutrons transfer their energies to human tissue mostly through recoil protons from elastic scattering with hydrogen, whereas thermal neutrons undergo neutron capture reactions and generate γ rays within the body [12] that subsequently yield other charged particles. Through these indirect ionization interactions, neutrons can deposit enough energy to damage cells and cause mutations that may ultimately lead to a second cancer in the patient.

The residual activity in the machine [13], in the walls and even in the patient is also a concern. The unstable isotopes that remain after the emission of neutrons or after neutron capture have residual activities [14]. Activated materials with short half-lives do not contribute significantly to carcinogenic risk because they decay too quickly, nor do materials with long half-lives because they do not decay appreciably while the patient and staff are present. However, when the decay rate is high enough, the activated materials may present a radiation risk to the personnel involved in the treatment procedure.

The risks associated with neutrons vary significantly with the energies of the neutrons [12], as described by the energy-dependent neutron weighting factors published in the ICRP 103 report [15]. Fig 1.1 shows the ICRP neutron weighting factors as a function energy. Although these weighting factors are highly empirical and non-specific, they reflect how the carcinogenic risk associated with neutron radiation varies with energy. Therefore, in order to asses the biological risk of neutrons in a given situation, a good understanding of the neutron fluence spectrum is required.

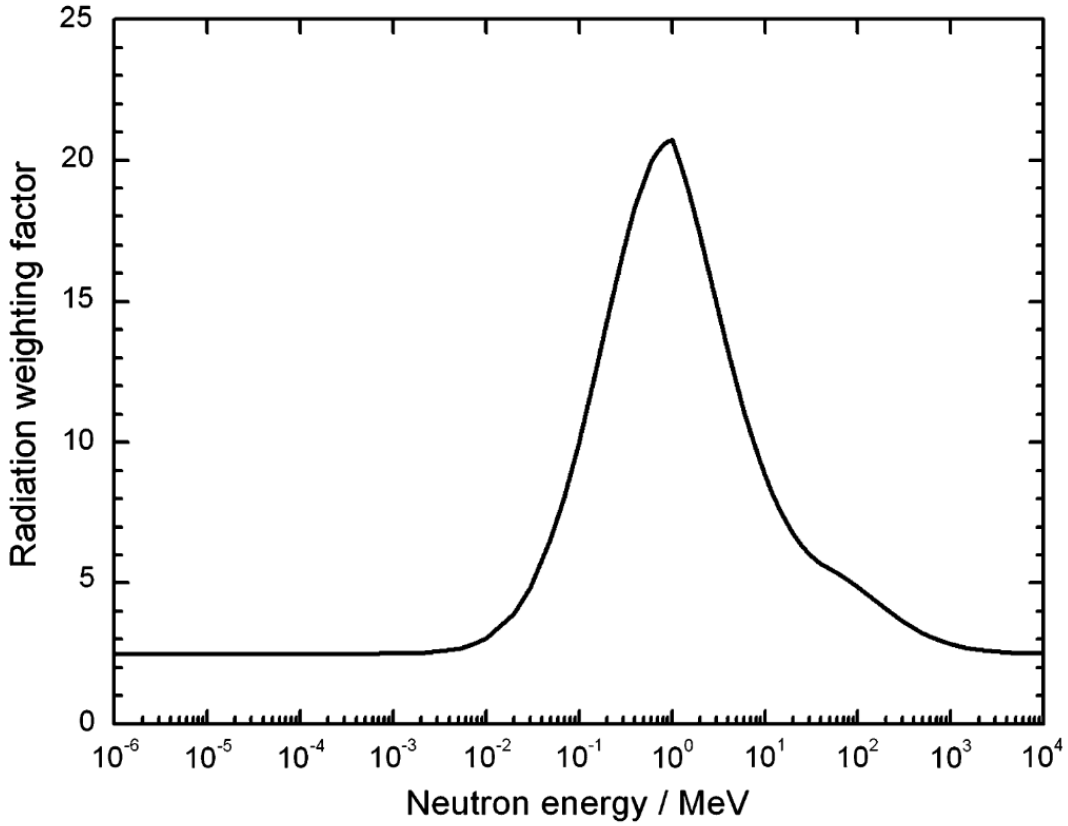

Figure 1.1 – The neutron weighting factors as a function of energy, for radiation protection purposes, as recommended by ICRP publication 103.

1.4 Neutron detectors

1.4.1 Active and passive detectors

Broadly, radiation detectors can be classified as active or passive detectors. Active detectors, such as ionization chambers, provide a measurement in real-time without the need to process the data. When an ion chamber is used, a charge or current measurement can be obtained from an electrometer immediately after or during its exposure to radiation. When using a passive detector, on the

other hand, an additional processing step is required to obtain a quantitative measurement. Some examples of passive detectors include the TLD dosimeter and gafchromic film detectors, both of which require a post-irradiation read-out process to obtain the dosimetric quantity of interest.

1.4.2 Neutron spectrometers

There are a wide range of neutron detectors, both active and passive, including gas-filled ionization chambers, proportional counters and bubble detectors, which can be used to measure neutron fluence. However, in themselves, these detectors lack the ability to discern neutrons with different energies. As discussed in Section 1.3.3, it is important to measure the fluence spectrum since the risks associated with neutrons changes as a function of their energies, and a neutron spectrometer is required to perform the task.

Two neutron spectrometers typically used in the radiation therapy context are the Bonner Sphere Spectrometer (BSS) and the Nested Neutron Spectrometer^{TM} (NNS). In this study, the NNS was used for all experimental measurements.

Bonner Sphere Spectrometer (BSS)

The Bonner Sphere Spectrometer consists of a thermal neutron counter and a set of interchangeable polyethylene moderator spheres, an example of which is shown in Fig. 1.2. Following the first description of a BSS by *Bramblett et al.* in 1960 [16], this spectrometer system has evolved into different variants. Multiple groups have investigated BSS systems with various active and passive thermal neutron detectors including $^{10}BF_3$ proportional counters, ^{3}He ionization chambers, SP9 counters and foils made of materials such as gold and indium [17]. Also, the number of moderator spheres has varied between different implementations.

Irrespective of the neutron detector used, the basic working principle of the spectrometer remains the same. The thermal neutron detector is located at the center of the moderator sphere and

(a) *(b)*

Figure 1.2 – The Bonner Sphere Spectrometer (BSS). (a) Photograph of a BSS during the spectral measurement [18]. Multiple spheres can also be seen in the picture. (b) Photograph of another BSS on a tripod under an electron linac [19]

the moderator, depending on its thickness, slows down neutrons to a detectable energy range for the detector. With moderator spheres of varying thicknesses, a wide range of neutron energies can be sampled in this manner. In addition to the polyethylene spheres, some systems utilize moderator shells of iron, lead or copper to extend the detectable neutron energy range to higher energies.

Nested Neutron Spectrometer (NNS)

The Nested Neutron Spectrometer (NNS) is shown in Fig. 1.3. This system consists of seven cylindrical moderator shells comprised of high density polyethylene (HDPE) and a ^{3}He ionization chamber as the thermal neutron detector [20]. The moderator shells are assembled in a Russian doll fashion around the thermal neutron detector. Practical aspects of this system are discussed in detail in Section 2.1.

(a) *(b)*

Figure 1.3 – The Nested Neutron Spectrometer (NNS). (a) Photographs of the 3He chamber, concentric moderator shells, and final assembly mounted on a tripod. (b) A schematic cross section of the NNS showing the 3He chamber at the geometrical center [21].

The NNS operates similarly to the BSS, except that the NNS cylindrical moderator shells are arranged inside one another whereas the BSS typically consists of several independent spherical moderators. The number of NNS shells can be chosen depending on the moderation required, which capitalizes on the benefits of the BSS while improving the practicality of the spectrometer system [20] by enabling the user to carry only the weight of the largest assembly.

The BSS was constructed with spherically-shaped moderators to ensure that the detector has a response independent of the direction of incident neutrons [20]. Thus, the dimensions of the cylindrical NNS moderators were carefully optimized to achieve a near angular isotropic response to neutrons and thereby making the NNS commensurable to the BSS in all domains.

Similar to the BSS, when measuring high-energy neutrons generated by a proton beam or a nuclear reactor, the NNS can be extended to higher energies by incorporating a brass moderator into the detector system [3].

1.5 Motivation for this research

The Nested Neutron Spectrometer in its default configuration works well in situations where the neutron fluence rate is low. This has been verified in the past using neutron sources with low decay rates, like Americium-Beryllium (Am-Be), and whose spectra are known [21][20]. But there is no well-characterized radioactive source with a high enough fluence rate to validate the conventional NNS behaviour at high fluence rates. It is assumed that the spectrometer is accurate when the neutron fluence rates are high, however this may not be true and there are no validations performed.

High neutron fluence rates are frequently encountered in radiation therapy, and the NNS has been used to measure these spectra [21] [22]. The accuracy of these studies and related work is somewhat uncertain until the assumption underlying the use of the NNS at high fluence rates is validated. Therefore, it is important to develop a method to verify that the NNS is indeed accurate at measuring neutron fluence spectra in high fluence rate environments. In this work, an indirect approach to ascertain the accuracy of the system is presented. We performed neutron spectrometry, in the context of radiotherapy, with a conventional and a new passive NNS to verify if they converge to the same spectrum.

The specific objectives of this validation study were as follows:

1. Develop a passive NNS system using gold activation foils that can be operated in high neutron fluence rates.

2. Formulate a workflow to perform the neutron spectroscopy with the passive NNS

3. Model the detector system and obtain the response functions of the passive NNS via Monte Carlo simulations.

4. Compare neutron spectra measured with the conventional NNS and the newly-developed passive NNS.

1.6 Overview of the thesis

This thesis is a comprehensive description of the steps involved to achieve the objectives listed above. The text is arranged in four chapters (excluding this introductory chapter).

In Chapter 2: Theory, the scientific concepts required for understanding the methods and results of this study are introduced. The conventional NNS, its functionality, the passive NNS and the theory behind the different facets of the workflow are discussed.

The technical details of modelling the passive detector system for generating the response functions, the procedure for performing a spectral measurement in a radiotherapy bunker and the activation analysis of gold foils are presented in Chapter 3: Methods.

In Chapter 4: Results and Discussion, all the results obtained after modelling, measuring and analyzing are presented. Also, a critical discussion on the resulting trends, characteristics and discrepancies is included in this chapter, followed by a discourse on the future work to be done.

In the final Concluding chapter, the significant features of this study are emphasized.

Chapter 2

Theory

2.1 The conventional Nested Neutron Spectrometer

The original configuration of the NNS, as provided by the vendor (Detec Inc, Gatineau, Quebec, Canada), has an active ^{3}He detector core and seven concentric moderator cylinders. Throughout this text, any reference to the conventional NNS will allude to this original configuration unless specified otherwise. In this study, the conventional NNS was modified to develop a passive system and comparisons have been drawn between the two. Therefore, it is important to understand the different working aspects of the conventional NNS before the modified passive NNS is introduced.

2.1.1 The active neutron detector

The main component of the conventional NNS is the ^{3}He detector core. The ^{3}He ion chamber is filled with 2 atm of ^{3}He gas and 0.7 atm of krypton as quenching gas [21]. With a neutron capture cross-section of 5330 barns for thermal neutrons, the ^{3}He gas atoms interact with neutrons when exposed to a neutron field, and undergo ^{3}He(n,p)^{3}H reactions [23]:

$$^{3}\text{He} + \text{n} \rightarrow {}^{3}\text{H} + \text{p} + 765\ \text{keV}$$

The 765 keV reaction energy is shared among the triton and proton released in the reaction. If a pulse-height spectrum is obtained from the ^{3}He counter, the kinetic energies collected from both these particles will manifest as an energy-peak in the spectrum. It is essential to understand that the peak is associated with the 765 keV, not with the energy of the incoming neutron. Therefore, by determining the counts corresponding to this energy peak, the number of ^{3}He(n,p)^{3}H reactions can be calculated, and by extension the number of neutron interactions but not their energies.

2.1.2 Response functions of the NNS

Detector response functions map how the sensitivity of a detector changes with particle energy, for example the number of neutron interactions in the detector per unit fluence. The sensitivity of the ^{3}He detector varies with neutron energy and is most sensitive to thermal energies. However, the NNS moderator shells change the sensitivity profile relative to the spectrum being sampled by selectively thermalizing higher energy neutrons. Therefore a set of response functions of the NNS is required, one for the bare ^{3}He chamber and one for each moderator configuration, in order to analyze the measured data.

The response functions of the NNS for all moderator shell configurations, as provided by the vendor, are shown in Fig. 2.1. The energy dependent responses were determined through Monte Carlo simulations, which are described in Section 2.5. These response functions were defined as the number of ^{3}He(n,p)^{3}H reactions per unit neutron fluence and were obtained after modelling the detector configurations using the MCNP Monte Carlo platform [24]. It can be seen in Fig 2.1 that, as previously discussed, the peak sensitivity shifts to higher energies as the moderator thickness increases.

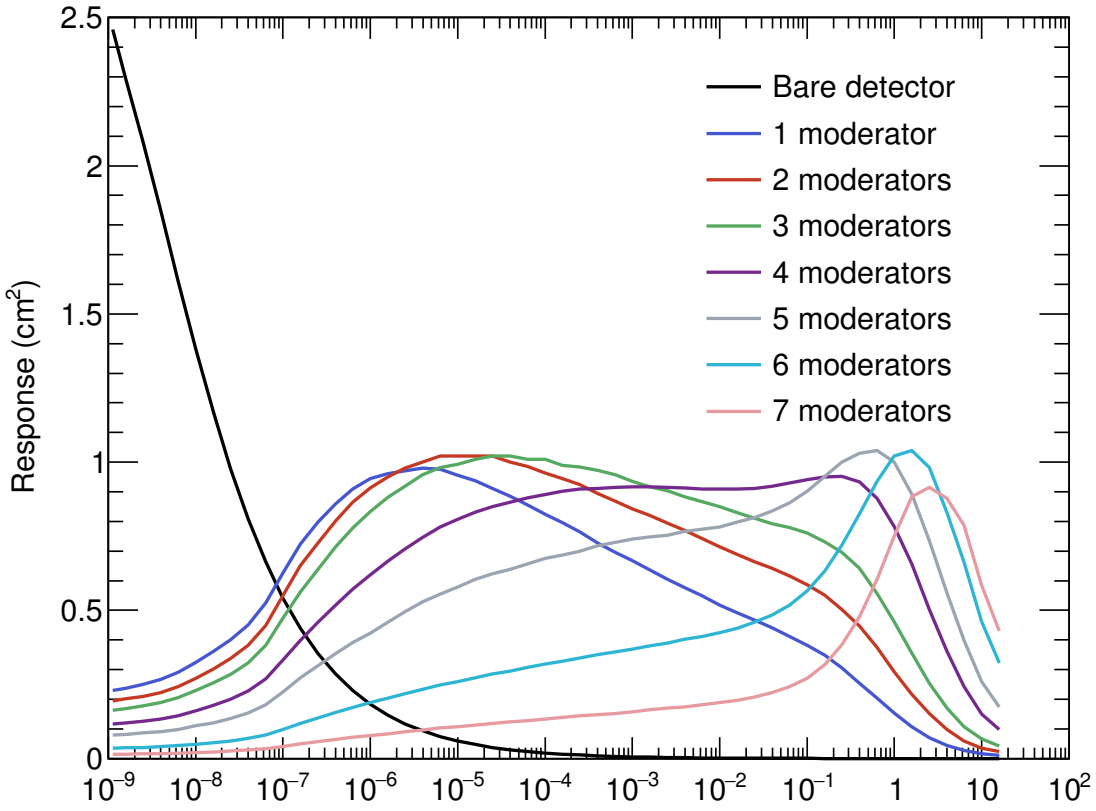

Figure 2.1 – The conventional NNS response functions for the bare ^{3}He detector as well as for all moderator configurations.

2.1.3 Operation modes of the NNS

The NNS can be operated either in pulse-mode (Fig. 2.2a), or in current-mode (Fig. 2.2b) [21]. In pulse-mode, the ^{3}He ionization chamber is connected to a pre-amplifier and the signal is fed into a multi-channel analyzer (MCA). From the pulse-height spectrum obtained with the MCA, the neutron fluence rate can be determined. However, pulse pileup occurs in high fluence rate environments wherein the maximum count rate of the MCA ($\sim$10,000 counts/s) is exceeded, resulting

in increased detector deadtime and causing the method to break down. Current-mode can be used to solve this problem since individual pulses are no longer counted.

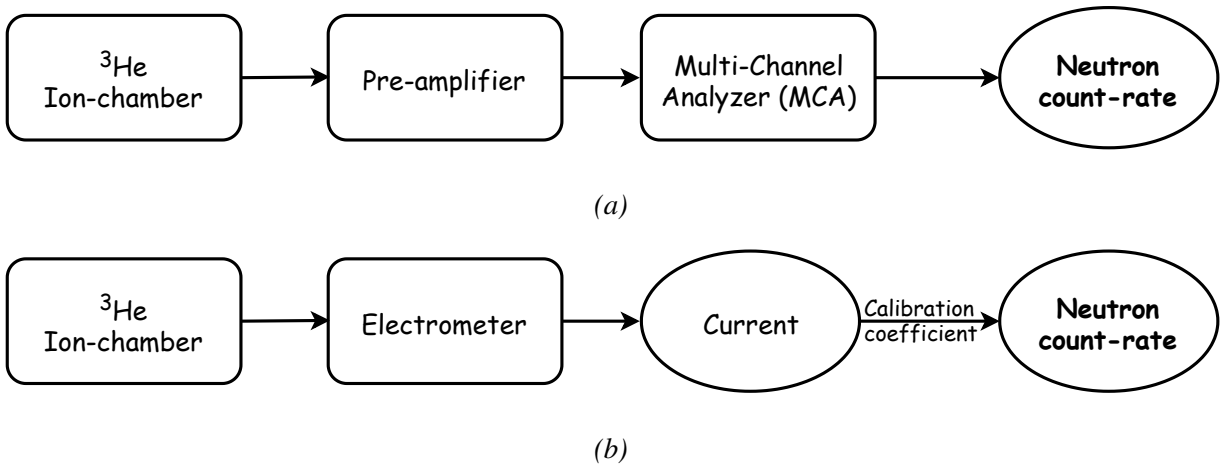

Figure 2.2 – The operational modes of the Nested Neutron Spectrometer: (a) The pulse-mode and (b) the current-mode

In current-mode, the ^{3}He chamber is connected to an electrometer, which can measure the total charge accumulated over the time of measurement and thus the time-averaged current. This current can be converted to the corresponding neutron count-rate using a calibration coefficient. An NNS calibration coefficient is equal to the ratio of the measured count-rate in pulse-mode to the measured current in current mode, when measurements are performed under the same experimental conditions in a low count-rate situation. Individual calibration coefficients for each moderator configuration of the NNS, and the average value used experimentally, are presented in Table 2.1.

Measurement in a mixed field

The ^{3}He detector is sensitive to photons as well as neutrons, which presents a problem when the photon background signal is significant compared to the neutron signal. In such scenarios, a ^{4}He is used in conjunction with the ^{3}He counter. The ^{4}He detector has the same photon response as the

Moderator	Pulse-Mode (counts/s)	Current-mode (fA)	Coefficient [fA/(counts/s)]
7	83.83	692	8.3
6	99.15	720	7.3
5	89.53	619	6.9
4	76.87	598	7.8
3	59.23	566	9.6
2	49.82	444	8.9
1	38.21	233	6.1
Average	-	-	7.8±1.2

Table 2.1 – Calibration coefficient for each NNS moderator configuration obtained using a 5 Ci Am-Be source at the neutron laboratory of the Canadian Nuclear Safety Commission (Taken from Maglieri et al. [21]).

^{3}He detector, but is insensitive to neutrons [20]. Therefore, it can be used to measure the photon background, which is subtracted from the total signal obtained from the ^{3}He chamber.

2.1.4 Need for a passive detector

The current-mode of the NNS system was developed because pulse-mode fails when the neutron count rate is higher than 10^4 counts/s. In a radiotherapy environment, for example when a linac is operated in 15 MV photon beam mode, the neutron count rate in the bare ^{3}He chamber exceeds 10^5 counts/s. Hence, it is ineluctable to use the detector in current-mode operation.

As discussed in the Section 2.1.3, in current-mode, the measurement of current is converted into count rate by means of the calibration coefficient. The underlying assumption behind this approach is that the count rate is linearly proportional to the measured current for all neutron

fluence rates. The linearity can easily be verified at lower neutron fluence rates, by obtaining measurements in both pulse-mode and current-mode, as was done during the initial calibration of the NNS to determine the coefficients listed in Table 2.1. But at higher neutron fluence rates this is no longer a possibility due to the experimental limitations of pulse mode. Therefore, in this project a passive NNS system was developed in order to verify the accuracy of the conventional NNS at high neutron fluence rates for which pulse mode cannot be used.

2.2 A passive NNS with gold foils

The conventional NNS has an active ^{3}He detector core that can be replaced with a passive detector to yield a passive NNS system. A common class of passive detectors used for neutron counting are activation foils. There are many different material choices for activation foils including gold, indium, and dysprosium [25].

2.2.1 Requirements of an activation foil

For neutron studies, activation foils with the following characteristics are preferred [26]:

1. There should be a possibility to perform a spectroscopic analysis on the radioactive sample. This implies, that the radioactive decay must lead to the emission of a gamma ray, which can be detected using a spectrometer.

2. The branching ratio in the decay leading to the emission of a gamma ray should be sufficient to obtain high gamma yield.

3. The decay scheme of the radioactive isotope should be simple and well defined. It should have a unique stable isotope for which high purity samples are available.

4. The half-life of the corresponding radioactive isotope should be neither too short nor too long. If it is too short, then the spectroscopic analysis must be performed immediately after irradiation. If it is too long, then the analysis has to be performed for a longer duration to get a significant measurement.

2.2.2 Gold activation foil

In our study, we modified the conventional NNS by replacing the active ^{3}He chamber with gold activation foils. Gold fulfills the requirements listed in Section 2.2.1, is widely used in low-energy neutron detection studies [27], and was thus chosen as our activation foil material. It also has a unique stable isotope, ^{197}Au, which can be obtained with high purity albeit at high cost.

When neutrons bombard the gold foil, they are captured and the stable gold isotope changes to a radioactive one through the reaction ^{197}Au(n,γ)^{198}Au. The neutron capture cross-section of ^{197}Au is plotted against the incident neutron energy in Fig 2.3, and capture peaks can be observed near the thermal energies.

The radioactive gold isotope: ^{198}Au

The neutron activated gold isotope, ^{198}Au, has a half-life of 2.696 days [29] and a simple decay scheme that is shown in Fig 2.4. The unstable ^{198}Au nucleus undergoes β^{-} decay [30]; transforming into an ^{198}Hg isotope and emitting an electron in the process. Although there are three different pathways in the decay scheme, the decay to the excited state of ^{198}Hg, which has a Q value of 412 keV, is predominant over the other two with a branching ratio of 0.955 [31]. With the emission of a 412 keV gamma ray, the excited ^{198}Hg isotope relaxes into its stable ground state.

Gold matches well with the requirements mentioned in Section 2.2.1, which makes it suitable to use for our purposes. There is a possibility to perform a spectroscopic analysis on the ^{198}Au isotope because its decay involves the emission of gamma rays. Also, the branching ratio is sufficiently

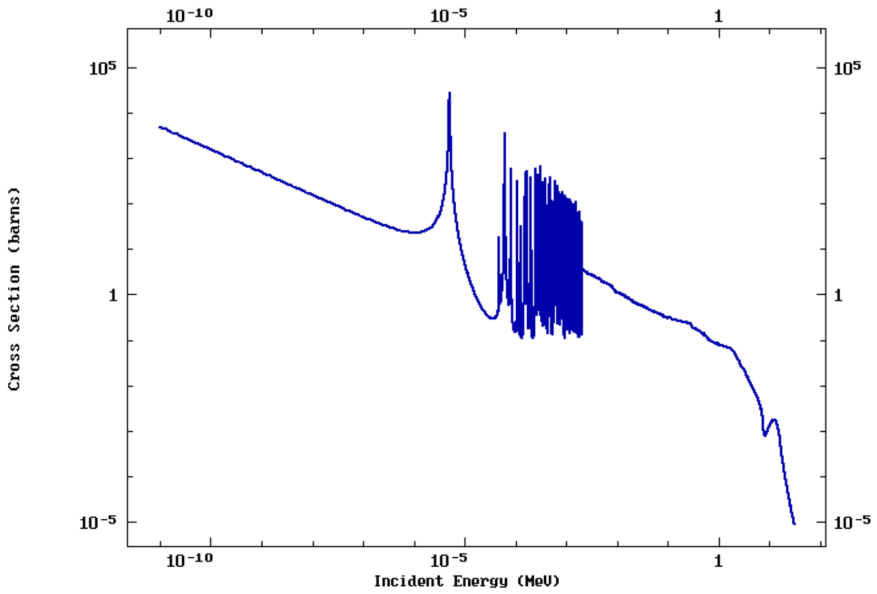

Figure 2.3 – The neutron capture cross-section of ^{197}Au isotope as a function of neutron energy. The figure was obtained from the ENDF cross-section database [28]

large to get a high yield of gammas. The decay scheme, which is simple and well defined with a unique stable isotope, is also an advantage to work with. Importantly, the half life of the ^{198}Au isotope, being almost three days, is a long enough window to perform the spectroscopic analysis with sufficient photon counts.

Photon activation of gold foils

Gold is not only sensitive to neutrons, but also to photons. When the ^{197}Au isotope of gold is exposed to a photon beam with energy above 8 MeV, photon activation takes place. High-energy photons interact with gold according to the reaction: ^{197}Au(γ,n)^{196}Au and form ^{196}Au isotopes [32], which differ from the ^{198}Au products of neutron capture. The 6.2 day half life of ^{196}Au is rather long compared to ^{198}Au and its decay involves the emission of gamma rays with energies of 333, 356 and 426 keV [33]. These can be distinguished from the neutron activated gold signal

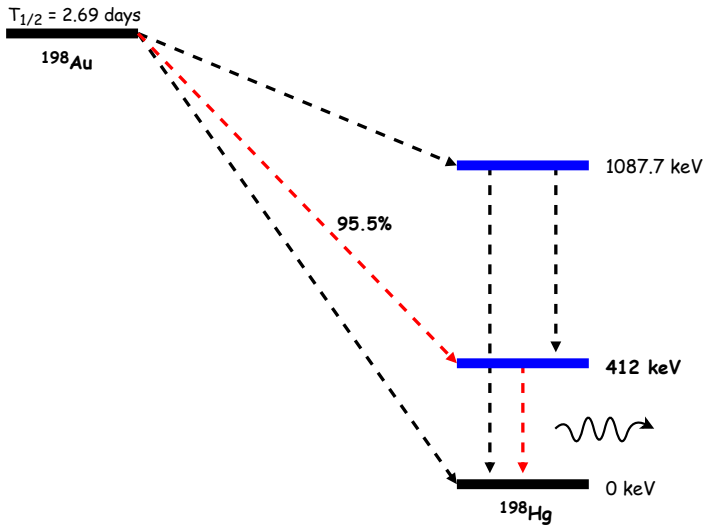

Figure 2.4 – The decay scheme of the unstable ^{198}Au isotope. The excited states of ^{198}Hg are colour coded in blue and the decay pathway of interest is shown in red.

during spectrometric analysis and hence, the effects of neutrons alone can be analyzed without using a separate detector for photon signals.

2.3 Activation analysis

The term activation analysis is often used as an abbreviation for Neutron Activation Analysis (NAA) [34]. It is a technique in which neutrons are directed onto a material sample to make it radioactive, and with a subsequent spectrometric analysis, the elemental compositions are identified. In this text, the term activation analysis does not correspond to the same technique. Here, activation analysis refers to the spectrometric analysis performed on the radioactive high purity gold foil in order to quantitatively measure the induced radioactivity of the sample.

As described in the previous section, the radioactive ^{198}Au isotope undergoes β^- decay, which involves the emission of an electron, and relaxation with the release of a gamma ray. Therefore,

either by the detection of the emitted electron or the gamma ray, one can measure the radioactivity of the foil. There are instances of beta counting [35] with neutron studies performed using the BSS with gold foils, but gamma spectrometry is more common because gamma rays undergo less self-absorption within the foil and thus are more efficiently detected by the spectrometer.

2.3.1 Gamma ray spectrometry

A gamma ray spectrometer is a device that can measure the gamma-ray spectrum emanating from a sample material. Depending on the resolution of the spectrometer, it can distinguish between photons of different energies and can count them individually. By counting the number of 412 keV gamma rays emitted by irradiated gold foils and accounting for the 95.5% branching ratio, the total number of neutron capture reactions can be inferred.

HPGe detector

Fig 2.5 shows the type of gamma ray spectrometer used in this study; a High-Purity Germanium (HPGe) detector and its associated components. The HPGe detector is essentially a reverse-biased diode made of a high-purity germanium crystal [36]. The depletion region formed in the crystal due to the reverse biasing acts as the sensitive volume for the radiation detection. When the gamma rays interact within the depletion region, electron-hole pairs are generated. A voltage bias introduces an electric field across the sensitive volume that drifts the electron-hole pairs across the depletion region and generates a detectable electric signal. This signal is amplified and analyzed with auxiliary electronic systems to produce the gamma-ray spectrum.

There are some important concerns to consider when using a high-purity germanium detector. (1) The high penetrating capability of the gamma rays requires a wide depletion region to ensure all their energies are deposited within the detector. One way to generate such a volume is to increase the purity of the germanium crystal as much as possible, which can be achieved using the zone

refining technique [37]. (2) The HPGe detector has a low band gap of 0.67 eV at 300 K, and the electrons in the valance band can easily escape to the conduction band with little kinetic energy. Hence, there will be noise associated with the HPGe detector, called leakage current, if operated at room temperature. Therefore, the HPGe detector is required to be operated under very low temperatures, and liquid nitrogen is used to maintain the temperature as low as 77 K during the detector application.

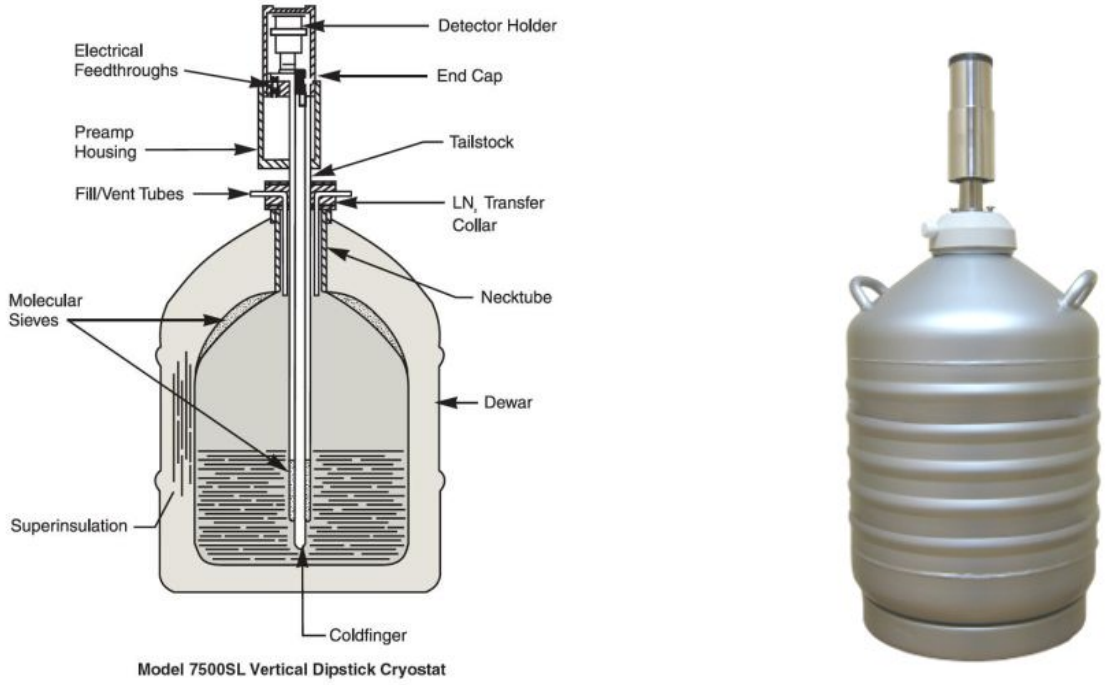

(a) *(b)*

Figure 2.5 – A High-Purity Germanium (HPGe) detector. (a) The schematic diagram of an HPGe detector [38]. The actual position of the sensitive volume within various other elements of the detector system is shown. (b) The photo of the HPGe detector in vertical configuration [39]. The vacuum capsule housing the sensitive volume can be seen on top of the liquid nitrogen dewar.

2.3.2 Specific saturation activity

The intent of measuring the radioactivity of the gold foil is to infer the number of neutrons that were incident on the foil during the time of irradiation. For every neutron that is captured, an ^{198}Au atom is created and eventually decays. Therefore, the total number of radioactive ^{198}Au atoms in the foil is equal to the number of neutrons captured.

Activity (A) is defined as the number of radioactive disintegrations per unit time, and is proportional to the number of radioactive atoms (N) present at that time [40]. Mathematically this can be expressed as:

$$A_t \propto N_t \quad and \quad A_t = \lambda N_t$$

where, λ is the constant of proportionality, commonly known as the decay constant.

Activity is therefore a dynamic parameter that decreases as the atoms decay away. For a simple decay scenario when the initial activity (A_0) of the sample is known and the sample is let to decay by its natural course, the activity decreases exponentially as shown in Fig 2.6. Thus, the activity of the foil at any time t (represented with A_t) can be expressed as:

$$A_t = A_0\, e^{-\lambda t}$$

In other words, if the activity at any time is known then the initial activity at time $t = 0$ can be calculated and subsequently the initial number of radioactive atoms can be obtained.

In the case of a neutron-irradiated gold foil, the decay does not follow the simple scheme since the irradiation is not instantaneous. Rather, the foil's activity profile changes as presented in Fig 2.7. Activity builds up from zero during the irradiation but is tempered slightly by simultaneous competing radioactive decay. Eventually, if irradiated long enough, the activity increases to a maximum value called the saturation activity (A^{∞}) and ceases to increase any further. This happens when the rate at which the foil is being activated (neutron capture rate) becomes equal to the rate

Figure 2.6 – The exponential decay curve of a radioactive sample with an initial activity A_0. The curve can be represented by the function $e^{-\lambda t}$.

at which the decay is happening (activity). Therefore, if we can calculate the saturation activity of the foil, we can determine the neutron capture rate that the foil was experiencing at the time of irradiation. When the irradiation is stopped, the decay continues in an exponential manner as per the case for the simple scheme discussed before.

If the gold foil was irradiated for a time t_i, and the gamma ray spectrometry occurred during a time t_m after waiting for a duration of t_w post-irradiation, then the specific saturation activity (saturation activity per unit mass) can be obtained using the equation [26] [31]:

$$A_s^{\infty} = \frac{\lambda \, (C_{measured} - B) \, e^{\lambda t_w}}{m \, q \, \varepsilon \, (1 - e^{-\lambda t_i}) \, (1 - e^{-\lambda t_m})} \tag{2.1}$$

where:

λ is the decay constant of ^{198}Au

$C_{measured}$ is the total counts of 412 keV gamma rays detected by the HPGe detector

B is the correction for dead-time and background signal of the HPGe detector

m is the mass of the activated foil

q is the branching ratio of ^{198}Au yielding 412 keV gamma rays

ε is the detection efficiency of the HPGe detector.

The derivation of this equation is provided in Appendix A.

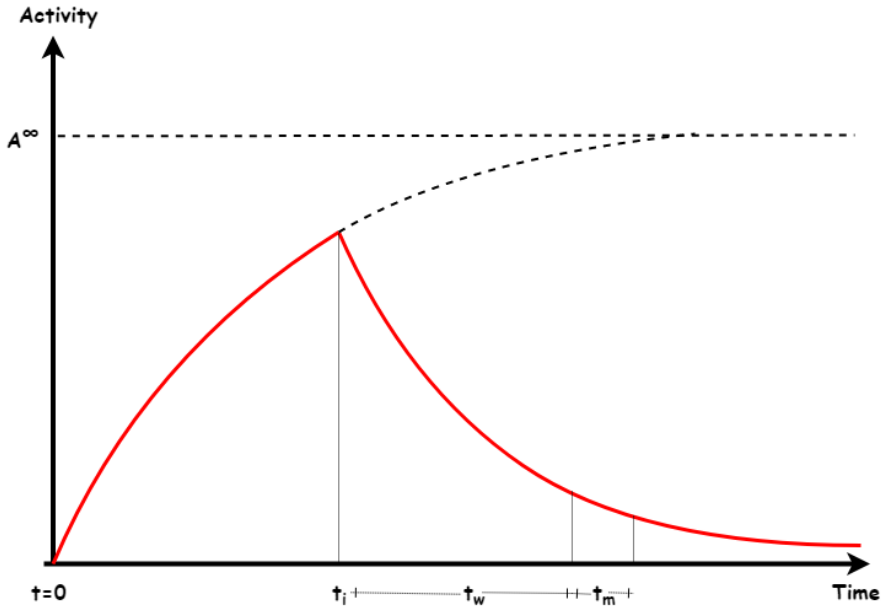

Figure 2.7 – The radioactivity profile of a gold foil during the time of irradiation (t_i), during the time of activation analysis (t_m) and the waiting duration in between (t_w). The saturation activity (A^∞) is shown with a dashed line.

2.4 Response functions of a passive NNS

Calculating the specific saturation activity of the foil only provides the number of neutron-capture interactions that happened in the gold foil. However, the total number of neutrons reaching the

the detector as a whole, at the point of measurement, is higher. The neutron fluence at a point in space is perturbed when the detector system is introduced. If we consider one configuration of the passive nested neutron spectrometer, consisting of a fixed number of moderator shells and the gold foil, we can imagine that some neutrons are scattered, some are attenuated in the moderator, some pass through the detector without interacting and only a fraction are captured in the foil.

Response is a parameter that relates the number of neutron captures to the total neutron fluence experienced in the absence of the detector. In this study, the response of the passive NNS with gold foils was defined as the number of neutron capture reactions per unit neutron fluence and per unit mass of foil:

$$Response(E) = \frac{No.\ of\ Neutron\ capture\ interactions(E)}{Neutron\ fluence(E)\ \times\ mass\ of\ the\ foil} \tag{2.2}$$

2.5 Monte Carlo simulations

Determination of the response functions through analytical calculations is almost impossible, especially because neutron interactions within the NNS are stochastic in nature [41]. The Monte Carlo (MC) method is a numerical tool that was developed in the 1940s for probabilistic calculations of various parameters for events that follow a probabilistic distribution. It estimates numerical quantities using randomized mathematical methods [42].

With Monte Carlo, the physics of radiation transport can be analyzed by simulating radiation interactions according to the relevant cross sections. The detector or the environment can be described by specifying its material composition and geometry, and various boundary conditions can be specified. Monte Carlo can track each individual particle and its interactions within a region of interest, and record parameters specified by the user. Some notable parameters for medical physics applications include the energy deposited by the particle, the particle fluence in a region, the number of secondary particles generated, track lengths and so on. With a large number of repeated simulations of individual particles, Monte Carlo is able to probabilistically predict the expected

values of these parameters.

As can be seen in the equation 2.2, there are two parameters that need to be determined through Monte Carlo simulations; the number of neutron capture interactions per unit foil mass and the neutron fluence. To determine the neutron fluence, it is important to understand how fluence should be defined in the Monte Carlo environment.

2.5.1 Fluence

Fluence or particle fluence is defined as the number of particles crossing an infinitesimal sphere centered at a point of interest, per unit cross-sectional area [43]. That is, if N is the number of particles striking a finite sphere around the point of interest, and *da* is the area of the great circle (the biggest circle that can be inscribed in a sphere) of an infinitesimal sphere around the same point, then the fluence (ϕ) is defined as :

$$\phi = \frac{dN}{da} \tag{2.3}$$

which has units of m^{-2} or cm^{-2} [44].

It is worth noting, that the planar fluence, defined as the number of particles crossing a fixed plane in either direction (scalar sum) per unit area of the plane, is not same as the fluence.

Alternative definition of fluence

Starting from the basic definition of fluence, an alternative definition of fluence was proven by Chilton [45] [46] and is stated as follows:

> *The Fluence at a point P is numerically equal to the expectation value of the sum of the particle track lengths (assumed to be straight) that occur in an infinitesimal volume dV at P, divided by dV.*

The above statement was shown to be true for isotropic as well as non-isotropic fields irrespective of the shape of the volume [44]. Therefore, the average fluence in a region is the sum of particle track lengths in the region divided by its volume. This alternative definition of fluence is used for calculating dosimetric parameters of interest in many Monte Carlo codes [47], and was implemented to score fluence in this project.

2.5.2 Variance reduction techniques (VRTs)

Even with modern computational capabilities, it is sometimes impractical to obtain statistically significant results using Monte Carlo in a reasonable amount of time when physical processes are allowed to occur according to their natural probabilities [42]. Variance reduction techniques (VRTs) have been developed to improve the statistical efficiency of a Monte Carlo simulation without affecting its accuracy or introducing bias. VRTs are different from so-called "speed-up techniques", which are approximations used to increase the speed of the simulation.

Geometry splitting and Russian roulette

Geometry splitting and Russian roulette are among the most simple, stable and reliable VRTs [48]. In geometry splitting, also known as particle splitting, replicas of a given particle are made to increase the probability of interaction within a certain region and thereby force the occurrence of an event. In order to avoid biasing due to the forced interactions, each particle is inversely weighted by the number of times it has been split [42].

Tracking individual particles after a geometry split can be computationally demanding due to the sheer number of particles. Because of this, geometry splitting is often followed by the Russian roulette technique. In this VRT, particles are selectively eliminated by terminating their transports based on a survival probability assigned to them, because it is computationally inefficient and irrelevant to continue tracking particles that lose their remaining energies outside the region of

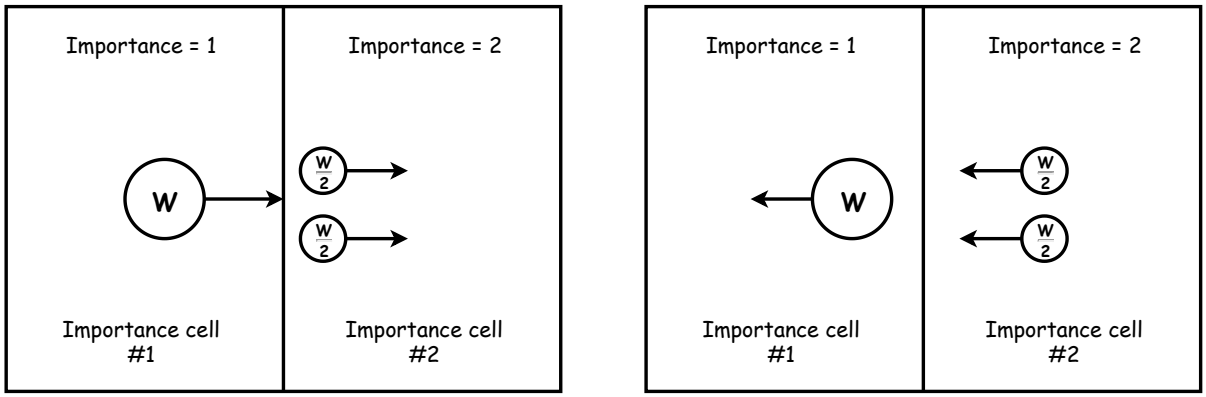

(a) Geometry splitting *(b) Russian roulette*

Figure 2.8 – Diagrams representing the two variance reduction techniques: (a) Geometry splitting and (b) Russian roulette. When particles move across the boundary of two regions of different importance, they split (geometry splitting) or get removed (Russian roulette) and the particle weight is modified accordingly.

interest. Russian roulette plays a game of chance on the particles that move away from the region of interest and it terminates the tracks that are not significant for the simulation. A representation of these VRTs is shown in Fig 2.8.

2.5.3 GEANT4

A variety of platforms are available to perform Monte Carlo simulations. Examples include MCNP [49], Penelope [50], EGSnrc [51], and GEANT4 [52]. Among the four platforms mentioned here, both MCNP and GEANT4 provide neutron simulations, but in this study GEANT4 was preferred for our Monte Carlo modelling because of the flexibility offered by its object-oriented design.

GEANT4 was developed and is maintained by an international collaboration [53] and is implemented in the C++ programming language following the object-oriented approach [54]. It has a wide range of built-in physics models and geometries that can be chosen according to the user's

preferences.

2.6 Unfolding neutron fluence spectra

As discussed in Section 2.4, the response functions of a detector are essentially a description of the detector's efficiency as a function of energy. If we assume that the neutron fluence spectrum at the point of measurement is $\Phi(E)$, which is also a function of energy, we can express the measured specific saturation activity (A_s^∞) of the gold foil as follows [26]:

$$A_{s_i}^{\infty} = \int R_i(E)\, \Phi(E)\, dE \tag{2.4}$$

where i indicates the NNS moderator shell configuration, and $R_i(E)$ is the response function of the corresponding configuration as a function of energy. Equation 2.4 is a Fredholm integral of the first kind [55] and, with the NNS system, one can obtain eight similar equations corresponding to all eight detector configurations. By solving these equations for $\Phi(E)$, through a process called unfolding (i.e. deconvolution), we obtain the neutron fluence spectrum.

Practically it is not feasible to obtain a continuous neutron fluence spectrum without any interpolation. Often fluence is specified for discrete energy bins of a finite width, wherein the number of energy bins is limited by the resolution of the response functions. The response functions of the conventional NNS, as showed in Fig. 2.1, were obtained for 52 logarithmically-spaced energy bins in the energy range from 1 meV to 16 MeV. Therefore, using these response functions, we can only obtain a 52-bin spectrum, or in other words, we are trying to determine 52 unknown fluence values by solving the 8 integral equations. Inverse problems such as this, with insufficient information to analytically solve the equations, are called ill-posed problems [56]. There are numerical methods that can be used to solve such problems, including the Maximum-Likelihood Expectation-Maximization (MLEM) algorithm, which was used in the present research project.

2.6.1 Maximum-Likelihood Expectation-Maximization (MLEM)

The inverse problem of positron emission tomography (PET) image reconstruction is commonly solved using the Maximum-Likelihood Expectation-Maximization (MLEM) algorithm [57] that was first published in 1977 [58]. The same technique can be used to solve Fredholm integral equations of the first kind (2.4) and has been used by our research group for neutron spectrum unfolding with the NNS in the past [21] [22] .

The MLEM algorithm maximizes the likelihood of obtaining the specific saturation activity $A_{s_i}^{\infty}$ by iteratively reconstructing the underlying fluence spectrum ϕ.

$$\phi_j^{k+1} = \frac{\phi_j^k}{\sum_{i=1}^{I} r_{ij}} \sum_{i=1}^{I} r_{ij} \frac{A_{s_i}^{\infty}}{\sum_{j'=1}^{J} r_{ij'}\, \phi_{j'}^k} \tag{2.5}$$

In this equation, k is the number of MLEM iterations, i is the index that spans the number of NNS moderator configurations ($I = 8$) and j and j' are indices that span the number of energy bins over which the response functions are defined ($J = 52$). Different indices for J are used to indicate that they do not iterate simultaneously. Therefore, r_{ij} is the response of the i^{th} configuration of the passive NNS for the j^{th} neutron energy bin. Note that the user must specify an initial guess spectrum, ϕ_j^0 at the beginning of MLEM (ie, when $k = 0$). The final spectrum to which MLEM converges is dependent on this guess spectrum, and our group has previously validated the use of a step function for unfolding secondary neutron spectra in radiation therapy [21].

2.6.2 MLEM-STOP

As described above, MLEM is an iterative algorithm that reconstructs the neutron fluence spectrum that has the greatest likelihood to yield a given set of measured specific saturation activities [21]. However, MLEM will run indefinitely and induce random noise in the spectrum unless a stopping

criterion is provided that terminates unfolding after sufficient convergence to the most likely spectrum. A simple solution is to terminate the algorithm when a fixed number of iterations, which is specified by the user, is reached. But this form of termination is a subjective user-dependent approach that can result in termination of MLEM too early (insufficient convergence) or too late (too much noise).

One method developed by *Bouallègue et. al.* in 2013 to solve this problem in PET image reconstruction was to introduce a new method termed MLEM-STOP [59]. *Bouallègue et. al.* considered the following indicator function that is calculated at each MLEM iteration k:

$$\mathscr{J}^k = \frac{\sum_{i=1}^{I}(m_i - q_i^k)^2}{\sum_{i=1}^{I} q_i^k} \tag{2.6}$$

where m_i are the actual measurements and q_i^k are the MLEM-reconstructed measurements ($q_i^k = \sum_j^J r_{ij}\phi_j^k$) at each iteration. They demonstrated that this indicator function approaches $\mathscr{J}^k = 1$ when the reconstructed image closely resembles the simulated ground-truth.

Our research group found that the direct application of this approach was not suitable to use in neutron spectrum unfolding because the indicator function $\mathscr{J}^k$ does not always reach a value of 1, as is the case for PET image reconstruction. The problem arises due to the wide range of neutron fluence rates encountered in radiotherapy. It was solved by our group by introducing a dynamic threshold value for $\mathscr{J}^k$ (instead of 1); the details of which are described by *Montgomery et al* [60][61]. This modified MLEM-STOP method was adopted for the present work.

Chapter 3

Methods

The objective of this research project was to develop a passive Nested Neutron Spectrometer system and use it to obtain the neutron fluence-rate spectrum in a radiotherapy bunker. We sought to validate the accuracy of the active system in high neutron fluence-rate settings by comparing the performances of both the conventional NNS and the new passive NNS under the same experimental conditions.

This chapter discuss the various aspects involved in the development of the passive NNS, its operation, and analysis of the measurement data to produce the neutron fluence-rate spectra.

3.1 Developing a passive NNS

The passive NNS was built by modifying the original system, namely by replacing the ^{3}He detector core with gold foils. A variety of gold foils are available and it was important to carefully choose an appropriate thickness and purity.

In 2010, *Amgarou et al.* demonstrated how the response of the BSS system changes with gold foil thickness [48]. They observed a 3% drop in the detector response when the foil thickness was

increased by 10% and vice versa, which they explained was due to neutron flux depression and self-shielding [62]. The response also increases with the purity of the foil because the probability of a neutron interacting with the gold increases as the number of ^{197}Au atoms increases. Similar trends were expected from the gold foil of the passive NNS, and based on the results published by *Amgarou et al.* the foil was chosen to be thin (0.1 *mm* thick) and pure (99.99% ^{197}Au) [48].

3.1.1 Foil placement in the NNS

The NNS moderator shells have a hollow region at the center to house the cylindrical ^{3}He chamber. When the ion chamber is placed inside this cavity, its sensitive volume is centered at the geometric center of the entire device, for all moderator configurations. This point is specified as the point of measurement, and this is where the neutron fluence spectrum is specified. Thus, it was required that the gold foil of our passive NNS be placed at the same central position.

(a) *(b)* *(c)*

Figure 3.1 – The pictures of the acetal inserts that were made to fill the hole left by the ^{3}He chamber (a) the void inside the NNS moderator where the ion chamber is normally housed, (b) the ^{3}He chamber placed inside the moderator, (c) the acetal insert pieces, made to position the gold disc at the measurement location, shown next to the ^{3}He chamber.

To fill the void that was created when the ^{3}He chamber was removed, two cylindrical inserts were made out of polyoxymethylene (Acetal), with the same radius and a combined length equal to that of the ion chamber as shown in Fig 3.1. Small gold discs, also with the same radius (8 *mm*), were cut-out from the foil using a punching tool (Fig 3.2), and were placed between the inserts; one disc for each of the moderator configurations. With this setup, each gold disc was appropriately positioned inside the NNS with its face surface parallel to the flat surface of the moderator cylinders.

Figure 3.2 – The picture of gold discs that were cut-out from the gold foil using a punching tool.

3.2 Generation of response functions using GEANT4

The response functions of the passive NNS system were generated using GEANT4 (version 10.4, patch-2). Geant4 offers a variety of classes to handle modelling of the detector, particle transportation and scoring. Detector construction is a class in which the detector model can be made. A group of classes called action classes handle the various aspects of particle transportation. Scorer classes are used to tally various parameters of interest during the particle transport.

3.2.1 Detector modelling

The detector construction class of Geant4 has many built-in functions to aid the modelling of the detector. There are pre-defined solid geometries, a wide range of materials and elements in the Geant4 data base to assign different solids, and also the capability to combine different elements to create or modify various materials as required.

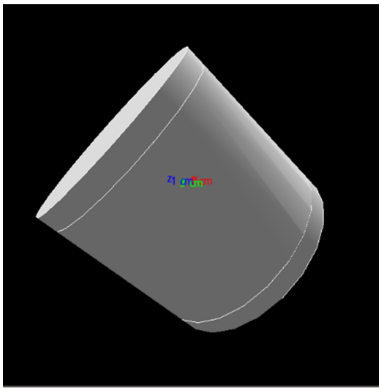

Figure 3.3 – The passive NNS model developed in Geant4

The particle tracking in the simulation was limited to a region of interest, called the mass world volume in Geant4 [63]. For our simulations, this world volume was defined as a 2 m radius sphere, at the center of which a model of the passive NNS was constructed. Construction of the NNS model was a two step process. The first step was to establish the geometry according to the known dimensions of the NNS, starting with the cylindrical moderator shells. A gold disc and the inserts that were used to center the gold foil were also generated and arranged appropriately in the mass world volume. The second step in the detector modelling was the assignment of appropriate material compositions corresponding to the geometries created. The gold disc was filled with the gold material readily available in the material data base while the polyethylene and the polyoxymethylene materials were custom created from basic elements for the moderator and the inserts respectively.

One important feature of the detector construction was the ability to allow flexibility in choosing the number of moderators to be used in the simulations. Since response functions were required for all 8 configurations of the passive NNS, the detector construction class was configured in such a way that the user can specify the number of moderators in the simulation using command line instructions. This significantly improved the usability of the simulation program.

3.2.2 Physics model

Many physics models spanning a range of energies are available in Geant4. In a radiotherapy bunker, we expect to see neutrons with energies as low as few meV up to the maximum energy of the radiation beam under consideration. Therefore, the QGSP_BIC_HP high-precision neutron physics model that has neutron cross-section data for energies up to 20 MeV was used in our simulation. The physics models in Geant4 obtain the neutron cross-section data from the G4NDL neutron data library distributed with the source code [64]. Note that the G4NDL library contains the same information as the standard ENDF-6 (it is the recommended evaluated nuclear data file for use in nuclear science and technology applications by the Cross Section Evaluation Working Group (CSEWG) of the United States.) data [65], but is formatted specifically for use in Geant4.

Investigations by *Mendoza et al* in 2014 showed that simulations performed with and without the thermal neutron scattering data were significantly different from one another [64]. In Geant4, the user has to explicitly evoke the thermal scattering and specify the corresponding interaction cross-sections. For this purpose, the QGSP_BIC_HP physics model was modified to incorporate the thermal neutron scattering data and the the corresponding thermal neutron scattering cross-section library. The elastic scattering data below 4 eV in the model were replaced with the thermal elastic scattering data in our simulation. The thermal neutron cross section data are limited to certain elements and have specific labels in the G4NeutronHPThermalScatteringNames class in Geant4. Therefore, the polyethylene and polyoxymethylene components of the NNS model were

defined using the thermal scattering compatible elements defined in the G4NeutronHPThermalScattering class.

3.2.3 Particle source

There are two classes in Geant4 that can be used to specify initial particle characteristics such as energy, distribution in space, and direction. These are the G4ParticleGun and G4GeneralParticleSource (GPS) classes. In our simulations, the GPS class was used to define the neutron sources because it provides greater flexibility to construct particle sources according to the user's specifications.

Individual simulations consisted of 10^7 monoenergetic neutrons that were distributed randomly on a cylindrical surface with a radius greater than the outer-most cylindrical moderator shell in each simulation. The direction of momentum of these particles was also random to achieve a perfectly isotropic neutron field. A unique simulation was performed for all 52 discrete energies, chosen at the center of the corresponding energy bins, over which the NNS response functions were to be defined (logarithmically spaced from 1 meV to 16 MeV), and for each moderator configuration.

3.2.4 Variance reduction

Neutron transport can be very slow especially when the moderators used are very thick because of the sheer number of complex interactions. We found it was necessary to implement VRTs to improve the efficiency of the simulations and to obtain statistical significance in a practical amount of computation time (12 days for the complete set of simulations with VRTs in our computer cluster).

The two VRTs described in Section 2.5.2 - geometry splitting and Russian roulette - were implemented in our simulation. Geant4 has a built-in geometrical importance sampling class that incorporates the two techniques. This geometrical importance class requires the user to delineate regions of importance in the simulation geometry (termed important cells) with varying importance

values assigned to each cell. When a neutron travels from a region of lower importance to a region of higher importance, particle splitting occurs such that the number of split particles depends on the importance assigned to that region. If the particle moves in the opposite direction, Russian roulette is performed and the tracks are selectively terminated based on their survival probability.

Geant4 allows the user to define a parallel world that is overlaid on top of the world volume. In this parallel world, different geometries can be defined without modifying the original mass geometry of the detector model. This functionality was used in our simulation to assign the importance weights to different regions. Specifically, we constructed concentric cylindrical importance cells of equal thicknesses, and centered at the center of the mass world volume. We assigned an exponentially increasing importance function from the outer-most cell to the innermost cell so that the particles split exponentially as they traversed through the moderator towards the gold foil.

3.2.5 Scoring

The simulations were performed to obtain two parameters of interest: (1) the number of neutron capture interactions per unit mass of gold and (2) the neutron fluence at the point of measurement. A region known as the sensitive detector in Geant4 must be defined in order to measure (score) these parameters. In our case, the gold foil geometry was assigned to be the sensitive detector.

(1) Capture score

Various scoring classes are available in Geant4 but to score the number of neutron captures per unit mass of the foil, a new class named the "nCapture scorer" was written and implemented in this work. For a single capture reaction, represented as ^{197}Au(n,γ)^{198}Au, multiple gamma-rays of various energies and an ^{198}Au isotope were created as secondary particles during the interaction. The nCapture scorer counted the number of ^{198}Au isotopes created during a simulation, which was equal to the number of neutron capture interactions that happened. By dividing the number

of ^{198}Au isotopes created by the mass of the gold foil, we obtained the first parameter required to calculate the response functions.

(2) Fluence score

As discussed in Section 2.5.1, Monte Carlo uses an alternative definition for fluence and in Geant4 this is implemented by way of the CellFlux scorer class.

It is essential to understand that we need to calculate the fluence at the point of measurement when there is no detector present. The detector introduces a perturbation to the fluence, and if we score the fluence in the presence of the passive NNS then we would measure a perturbed fluence score. To score the unperturbed neutron fluence an additional set of simulations was performed wherein all the geometries were filled with vacuum, including the gold foil geometry in which the fluence was calculated. The resulting response (the ratio of these two scores obtained) is the detection efficiency of our passive NNS, which describes how many neutrons are detected (neutron capture interactions) out of the total number of neutrons present (neutron fluence in air at the point of measurement).

3.2.6 An overview of the simulation process

The overall process of generating the response functions followed the steps given below:

1. A particular moderator configuration was chosen, and this configuration model was initialized in the detector construction class through command line instructions.

2. Using a macro file that specified the source parameters, the GPS source was initiated with a particular neutron energy.

3. After transporting the particles according to the indicated physics lists and with variance reduction techniques, the number of neutron captures per unit mass of the foil was calculated

and registered using the custom nCapture scorer.

4. The unperturbed neutron fluence at the point of measurement was calculated by modifying (eliminating) the detector material and repeating the simulation.

5. The ratio of the two scored parameters yielded the response of the passive NNS for that energy.

6. The energy of the incoming neutrons were then changed iteratively to calculate responses for all 52 energies chosen at the center of the corresponding energy bins.

7. Finally, steps $1-6$ were repeated for all moderator configurations, thereby iteratively generating the full set of response functions of the passive NNS.

3.3 The experimental measurements

The conventional NNS and the passive NNS were both used to perform the neutron fluence-rate spectrum measurements in a radiotherapy bunker at McGill University Health Centre (MUHC), Montreal. The point of measurement was 100 cm from the linac's isocenter along the treatment couch, as shown in Fig. 3.4.

The radiotherapy bunker was equipped with a Varian TrueBeam^{TM} STx linac (Varian Medical Systems, Palo Alto, CA). During irradiation, the gantry angle and the collimator angle of the linac were each set to 0 degrees, the collimator jaws were closed (field size of 0.5 $cm\times$ 0.5 cm), and the multi-leaf collimator (MLC) was fully retracted. All measurements with the conventional and passive NNS, were acquired using the 15 MV photon beam at a dose rate of 600 MU/min.

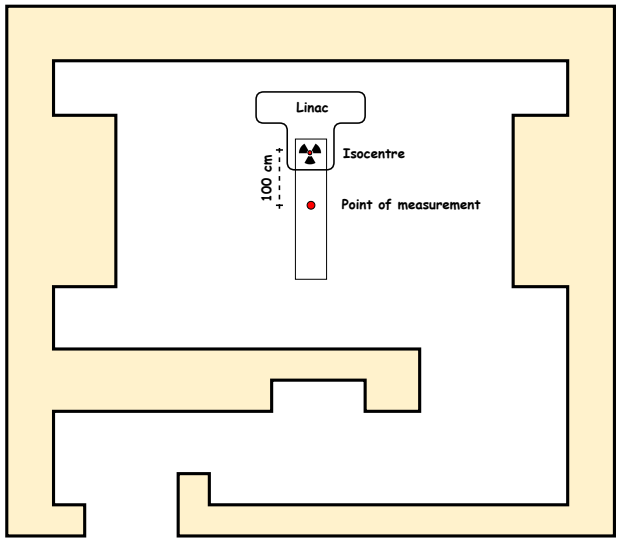

Figure 3.4 – Schematic diagram showing the point of measurement in one of the radiotherapy bunkers at the McGill University Health Centre (MUHC). Figure not to scale.

3.3.1 Passive NNS measurements

The passive NNS with all seven moderators was initially positioned on the treatment couch with the aid of the in-room lasers to ensure the central gold foil was located at isocenter. Then the couch was shifted 100 cm away from the isocenter, which accurately positioned the NNS at the desired measurement location.

Before performing the measurements, we estimated the expected foil activity for all moderator configurations using the generated response functions. In order to maximize the number of gamma-ray counts in the subsequent activation analysis, the passive NNS configurations were irradiated according to their expected activities; highest to lowest. To ensure that the vertical position of the gold foil in the NNS was constant, a unique non-moderating foam stand for each moderator configuration was placed under the NNS as shown in Fig 3.5.

With the aforementioned linac settings, each NNS configuration was irradiated for 15 minutes, making note of the start and end times. After each irradiation, the activated gold disc was extracted

from the NNS and stored in a labelled container. The NNS configuration was then changed; i.e. the number of moderators was modified, the corresponding foam stand was introduced and a new gold disc was placed inside. This process was repeated in the same manner for all configurations except for the bare detector, for which the experimental setup was unique.

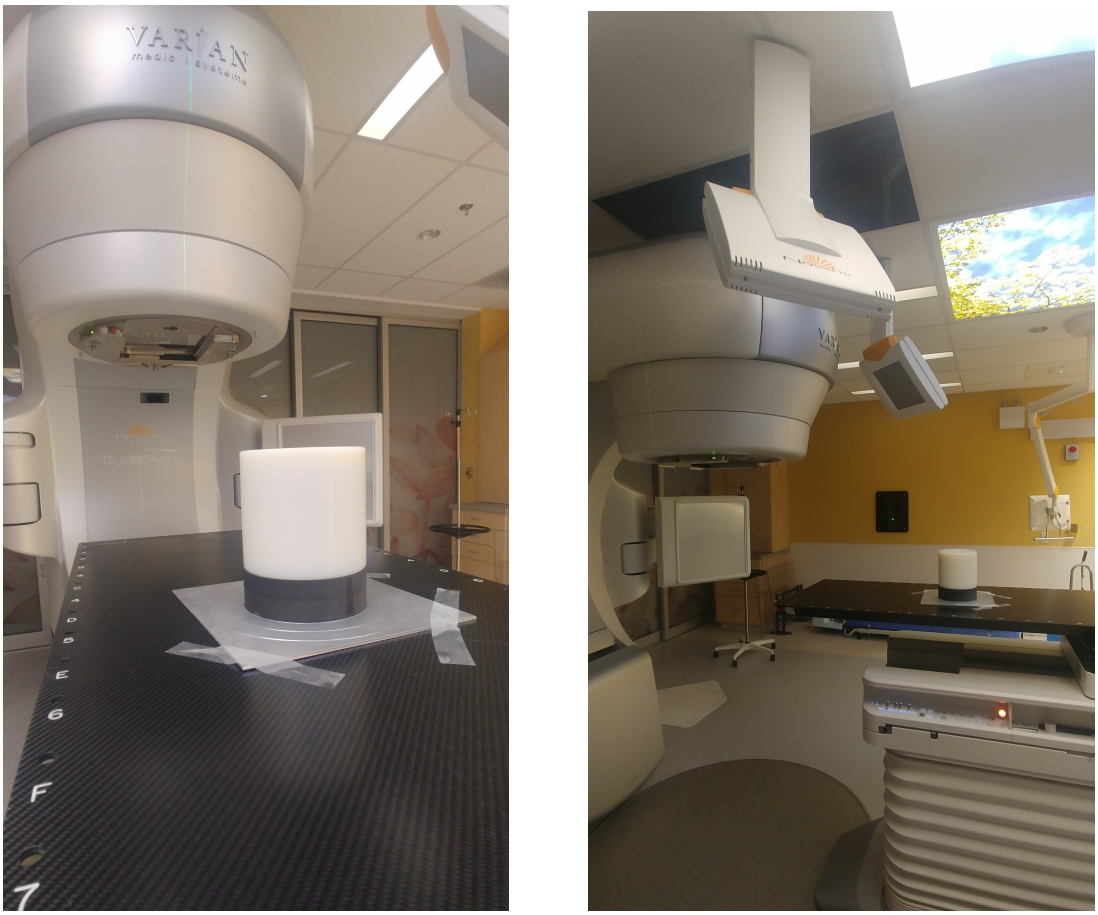

(a) *(b)*

Figure 3.5 – Photos of the experimental setup of the passive NNS in the 5-moderator shell configuration. (a) The NNS placed on the foam stand. (b) The passive NNS shown at the location of measurement.

In this case the foam was replaced with a metal stand that was provided with the conventional NNS to hold the bare ^{3}He chamber in position during irradiation. Using this holder and one of the

Acetal inserts, the foil was kept at the point of measurement as shown in Fig 3.6.

The estimate of the expected activity of the foil in this bare configuration was very low compared to the other configurations. Therefore, the bare foil was irradiated for 30 mins to increase the foil activity and thus improve the counting statistics during the subsequent activation analysis.

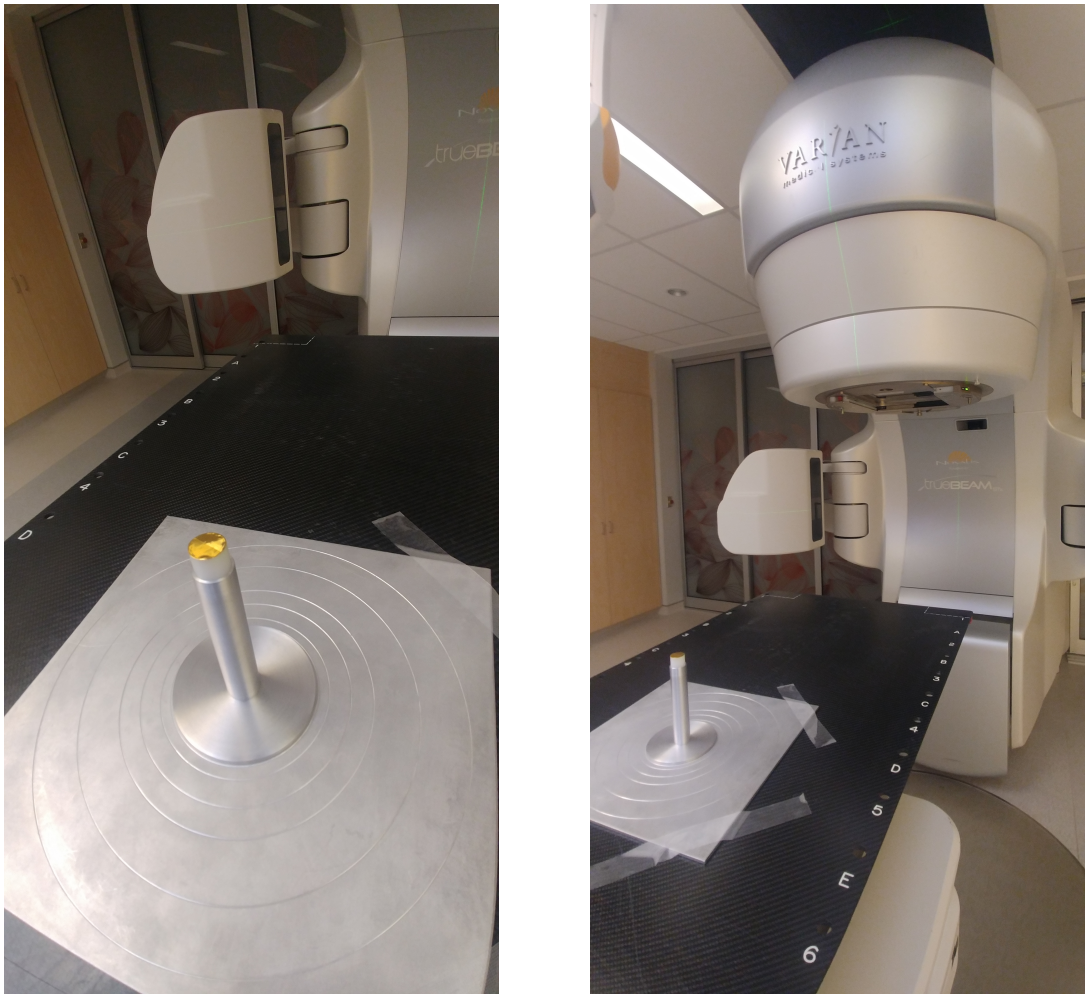

(a) *(b)*

Figure 3.6 – The experimental setup of the bare configuration of the passive NNS. (a) A gold disc placed in the ^{3}He detector holder. (b) Bare detector configuration at the measurement location.

3.3.2 Conventional NNS measurements

A set of measurements was also obtained using the conventional NNS for comparison purposes. The inserts and the gold discs where replaced with a ^{3}He chamber that was connected to an electrometer via a triaxial cable. Note that a biasing voltage of 150 V was applied to the chamber via the electrometer. Otherwise, the experimental setup was identical in terms of the detector position and the linac configuration. The measurements were performed for all the configurations of the NNS, starting with all seven moderators. Each moderator configuration was irradiated for 30 seconds after warming up the ^{3}He chamber, and the accumulated charges for each irradiation were recorded. Unlike for the passive NNS system, every irradiation was repeated three times and the results were averaged, which is a requirement of the MLEM-STOP method [60][61]. Subsequently the ^{3}He chamber was replaced with a ^{4}He chamber to measure the photon background. This background signal is relatively constant across all moderator configurations and therefore we only acquired measurements with ^{4}He for three configurations. Values for the remaining configurations were interpolated. The ^{4}He-measured photon backgrounds were subtracted from the ^{3}He-measured signals to determine the neutron signals.

3.4 Activation analysis

The spectroscopic analysis of the activated foils was performed using a HPGe-based ORTEC DSPEC Pro gamma-ray spectrometer system at the neutron activation analysis laboratory at the École Polytechnique de Montréal. The foils were analyzed as soon as possible the day after irradiation.

Gamma counting started with the gold foil that was expected to give the lowest measured activity in order to optimize counting statistics. The foils were carefully placed on top of a thin acrylic plate on the counting surface of the detector. The thickness of this acrylic plate can be

changed depending on the activity of the sample. For example, if the activity is too high, a thicker acrylic plate must be used to position the sample further away from the detector to decrease the risk of pulse pile-up and detector dead time. Once the foil was in place, the spectrometer was covered with lead blocks to eliminate any background contribution to the measurements. Fig 3.7 shows the experimental setup.

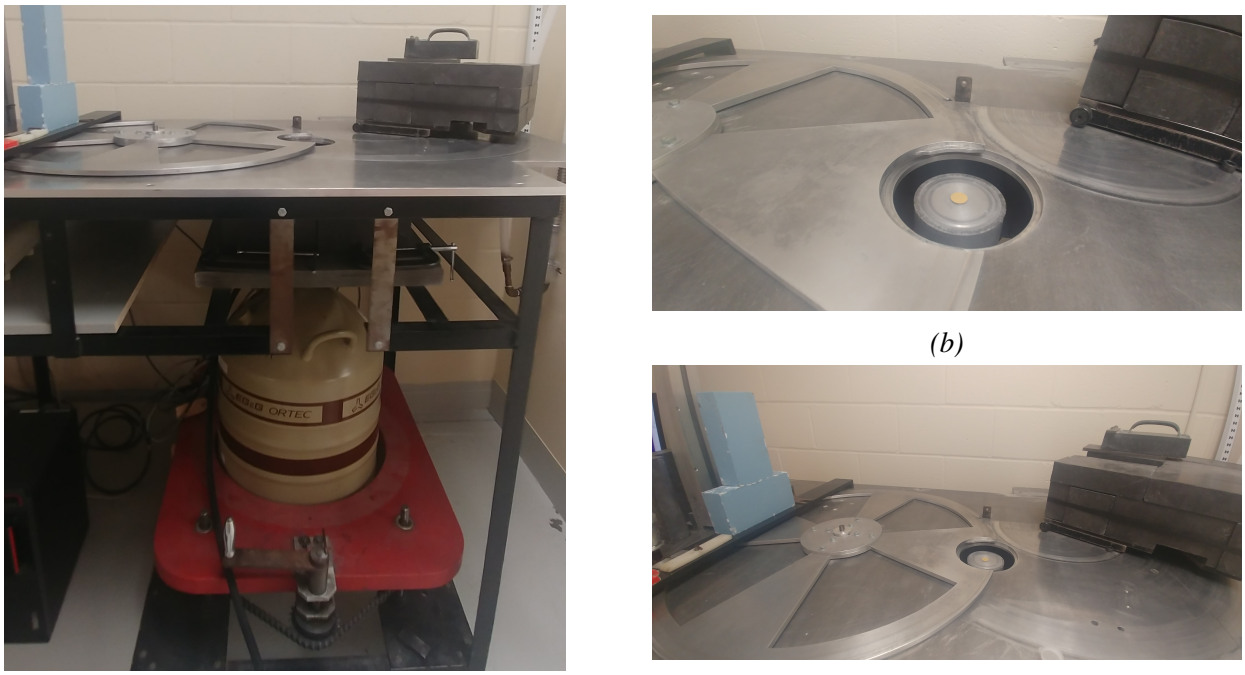

(a) *(b)* *(c)*

Figure 3.7 – The HPGe gamma-ray spectrometer used for activation analysis of irradiated gold foils. (a) the entire detection system, (b) the radioactive gold foil placed on top of an acrylic plate, (c) detection end of the HPGe system before covering with the lead blocks to attenuate background radiation.

Counting for each disc continued until at least 4000 counts were obtained in order to achieve reasonable statistics. The MAESTRO Multichannel Analyzer Emulation Software provided the spectrum, the gamma-ray count for the specific energy, live time (effective counting time corrected for dead time), and real time (duration for which the counting lasted) of the detector obtained

during the analysis. The times at which the counting started and ended were also noted alongside the masses of the activated foils measured using a weighing scale.

3.4.1 Spectrometer calibration

The detection efficiency of the gamma-ray spectrometer for 412 keV photons was specified by the HPGe vendor for only the thickest available acrylic plate. The following steps were taken to calculate the detection efficiency when the thin acrylic plate was used.

Two identical discs with the same dimensions as the gold discs were cut out from an aluminum sheet with 0.1% gold content. Both these foils were identically irradiated using the SLOWPOKE reactor at École Polytechnique de Montréal [66], which is typically used for neutron activation analysis (NAA). Both foils were expected to have the same activity, and their activities can be calculated using:

$$A = \frac{C}{\varepsilon \times \beta \times T\_live} \tag{3.1}$$

where:

C is the gamma count

ε is the detection efficiency

β is the branching ration of ^{197}Au and

T_live is the live time of the detector

One of the discs was counted on top of the thick acrylic plate and the other on the thin plate. If the counts (C), live time (T_live) and efficiency (ε) corresponding to the thick and thin plate are suffixed *thick* and *thin* respectively, we can write using equation 3.1

$$\frac{C_{(thick)}}{\varepsilon_{(thick)} \times T\_live_{(thick)}} = \frac{C_{(thin)}}{\varepsilon_{(thin)} \times T\_live_{(thin)}} \tag{3.2}$$

Using the known $\varepsilon_{(thick)}$ with the thick plate, the detection efficiency of the spectrometer with the thin acrylic plate ($\varepsilon_{(thin)}$) was calculated.

3.5 Unfolding

The conventional NNS measurements, which were averages of three repeat measurements, were unfolded using the modified MLEM-STOP method described in Section 2.6.2. The neutron count-rate measured with the ^{3}He chamber after removing the photon contribution was plugged into the MLEM-STOP algorithm along with the response functions of the conventional NNS provided by the vendor. Also in accordance with the MLEM-STOP protocol, a step function was inputted into the algorithm as an initial guess spectrum. The algorithm unfolded the raw measurements until an ideal iteration number was reached.

Performing multiple measurements with the passive NNS was not feasible because of the long irradiation times and the involved readout process. Therefore, the passive NNS measurements were unfolded using the conventional MLEM algorithm, which was terminated after 2412 iterations; i.e. the same number that was used for MLEM-STOP with the conventional NNS measurements, in order to facilitate comparison. To unfold the data obtained with the passive NNS, the saturation activity was calculated first. With the measurement of the irradiation duration, gamma counting duration and the waiting duration in between, the specific saturation activities of all the eight gold discs were calculated after plugging in the values obtained for background eliminated count, activated foil mass, detection efficiency, branching ratio and decay constant into equation 2.1. These saturation activities were then input into the MLEM algorithm. The simulated set of passive NNS response functions was used for unfolding these data along with the step function.

Chapter 4

Results and Discussions

4.1 Response functions of passive NNS

The response functions generated using our Monte Carlo simulations in Geant4 are shown in Fig 4.1. The data were discrete and were obtained for 52 energy bins but a smooth curve connecting them was generated for each moderator configuration to improve readability.

The response function of the bare detector has a significant low-energy peak which reflects the higher chances of neutron capture at thermal energies. As more moderators are added, a shift in this peak towards higher energies is observed, as expected. The moderators reduce the energies of the incoming high-energy neutrons to within a detectable energy range for the gold foil depending on their thicknesses; hence the peak shift.

4.2 Neutron fluence spectrum determined using the passive NNS

The neutron fluence-rate spectrum obtained after MLEM unfolding (for 2412 iterations) the measurements made using the passive NNS is plotted in Fig 4.2.

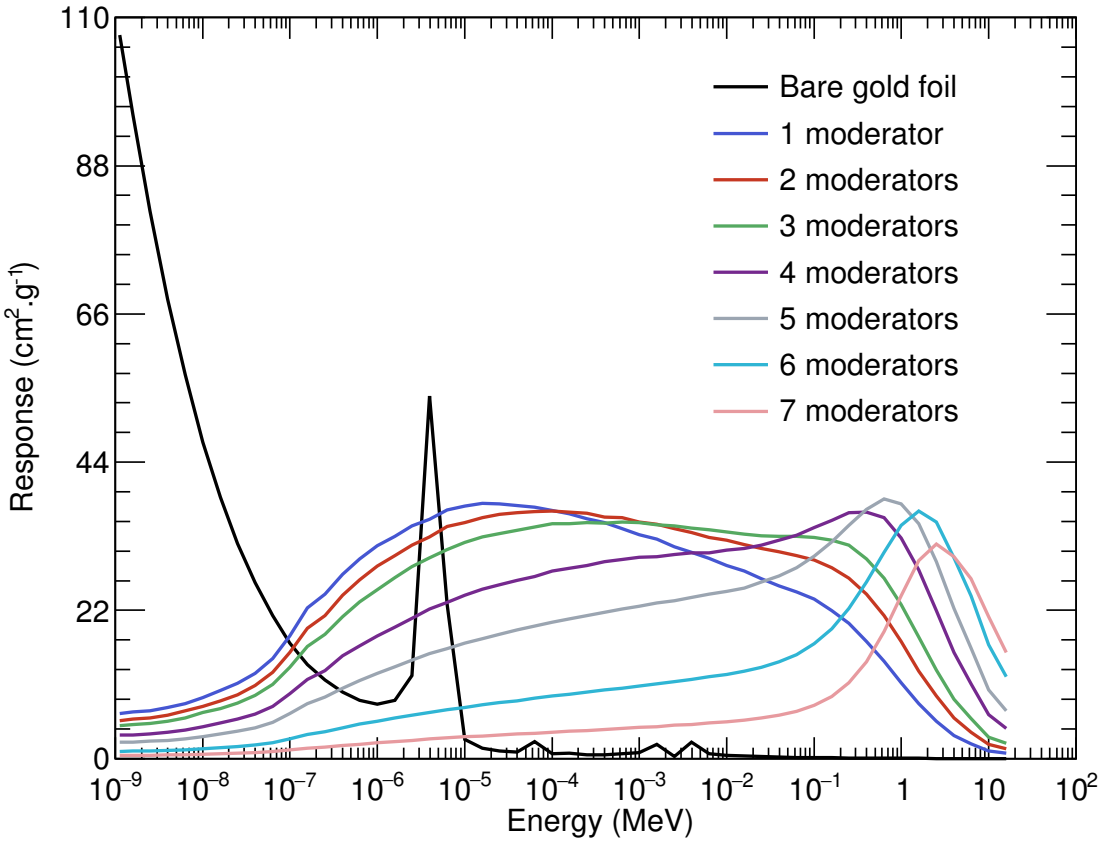

Figure 4.1 – The response functions of the passive NNS, generated using Monte Carlo simulations in Geant4. The response of the bare gold foil has a prominent peak at the thermal energies, which corresponds to an increased neutron capture cross-section that makes gold a thermal neutron detector.

There are two prominent peaks in the spectrum: A smaller peak at thermal energies (thermal peak) and a bigger peak around 1 MeV (fast peak). The fast peak corresponds to the neutrons created through evaporation processes and photoionization (as discussed in Section 1.3.1). In scenarios where a very high-energy photon/particle beam generates neutrons, like in a proton treatment facility, an additional distinct peak would be expected to appear at a higher energy due to photoion-

ization neutrons. Since we used a 15 MV photon beam for neutron generation, the photoionization peak is not distinguishable from the 1 MeV evaporation peak.

The thermal peak arises from the fast neutrons that lost their energies after multiple scattering in the bunker and the linac itself.

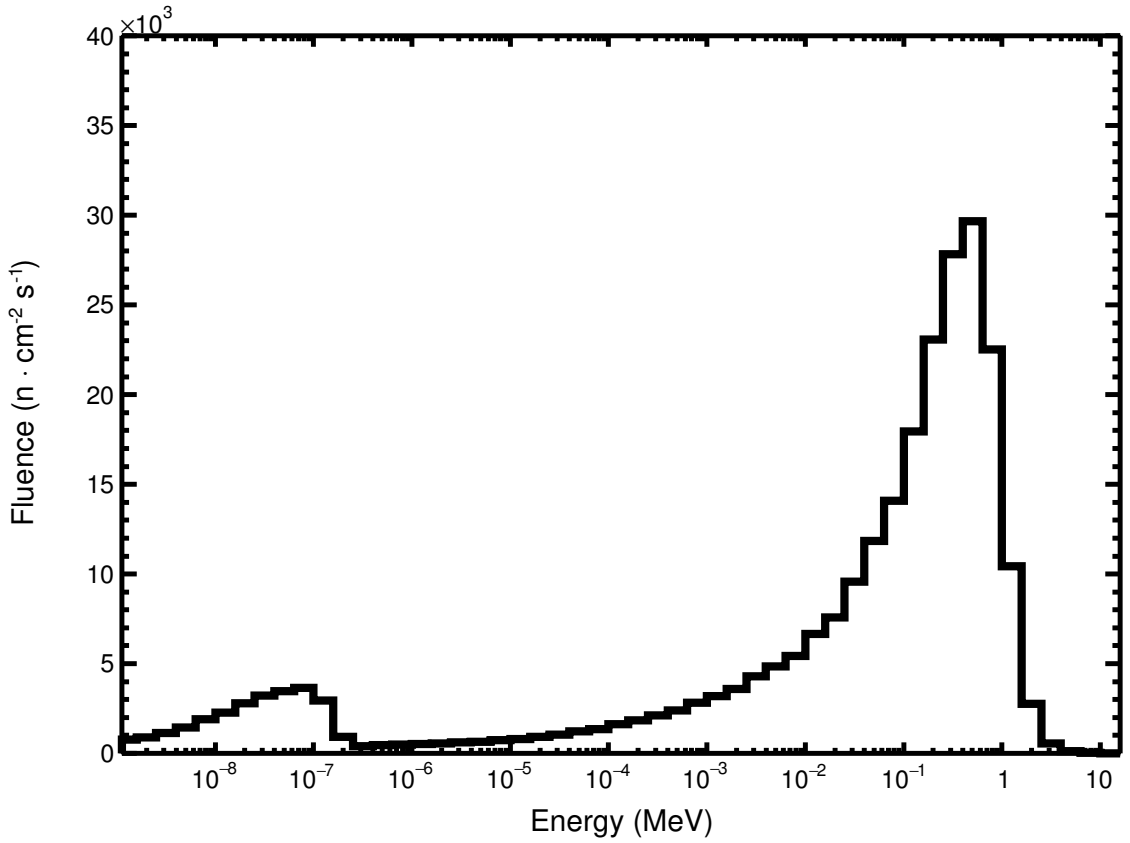

Figure 4.2 – The neutron fluence-rate spectrum generated by the 15 MV beam of a Varian TrueBeam linac at 100 cm from isocenter along the treatment couch and away from the linac. The spectrum was measured using the passive NNS and unfolded using MLEM.

4.3 Comparing the performance of the passive and active NNS

The neutron fluence-rate spectrum measured using the conventional NNS and unfolded using MLEM-STOP is plotted alongside the equivalent spectrum measured using our passive NNS in Fig 4.3.

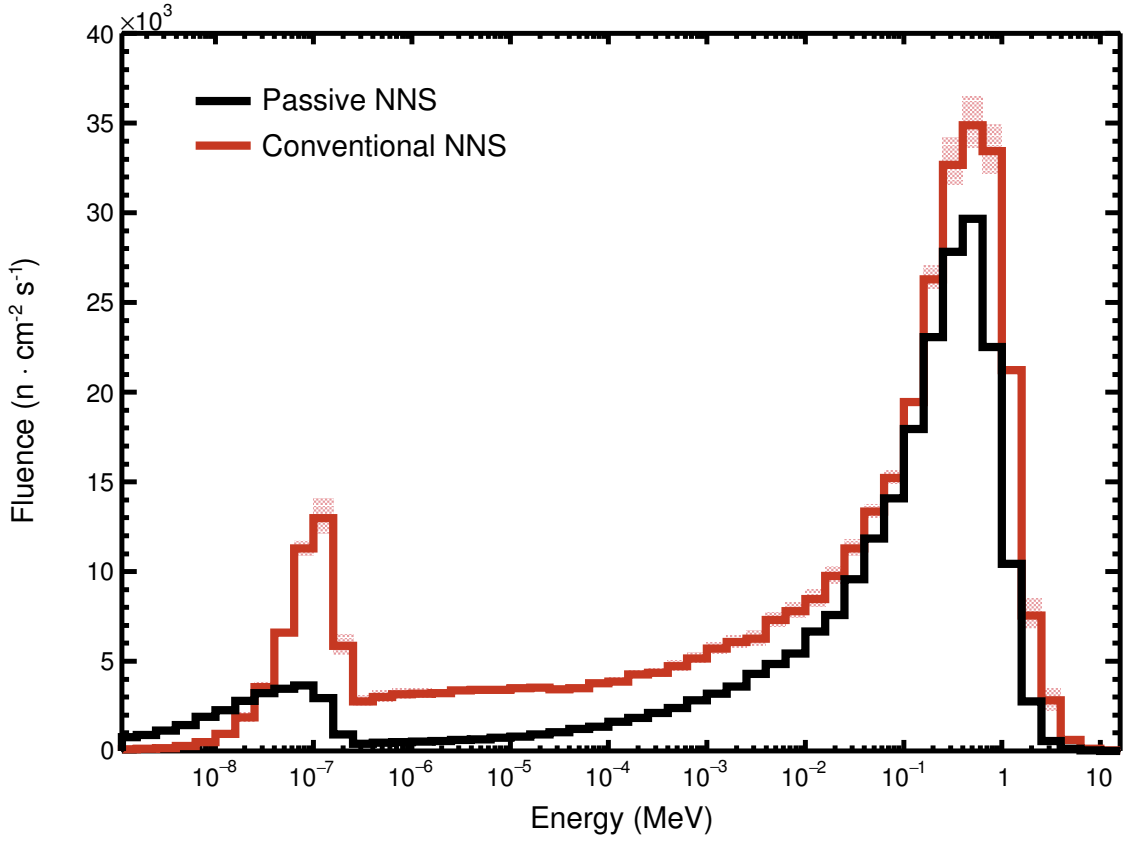

Figure 4.3 – Comparison of the neutron fluence-rate spectra obtained from the conventional NNS (red) and the passive NNS (black) obtained under the same conditions and for the same number of iterations (2412).

Overall, the spectra agree reasonably well with each other, particularly at the fast peak. However, there are prominent discrepancies in the height and location of thermal peak and the epither-

mal region of the spectra.

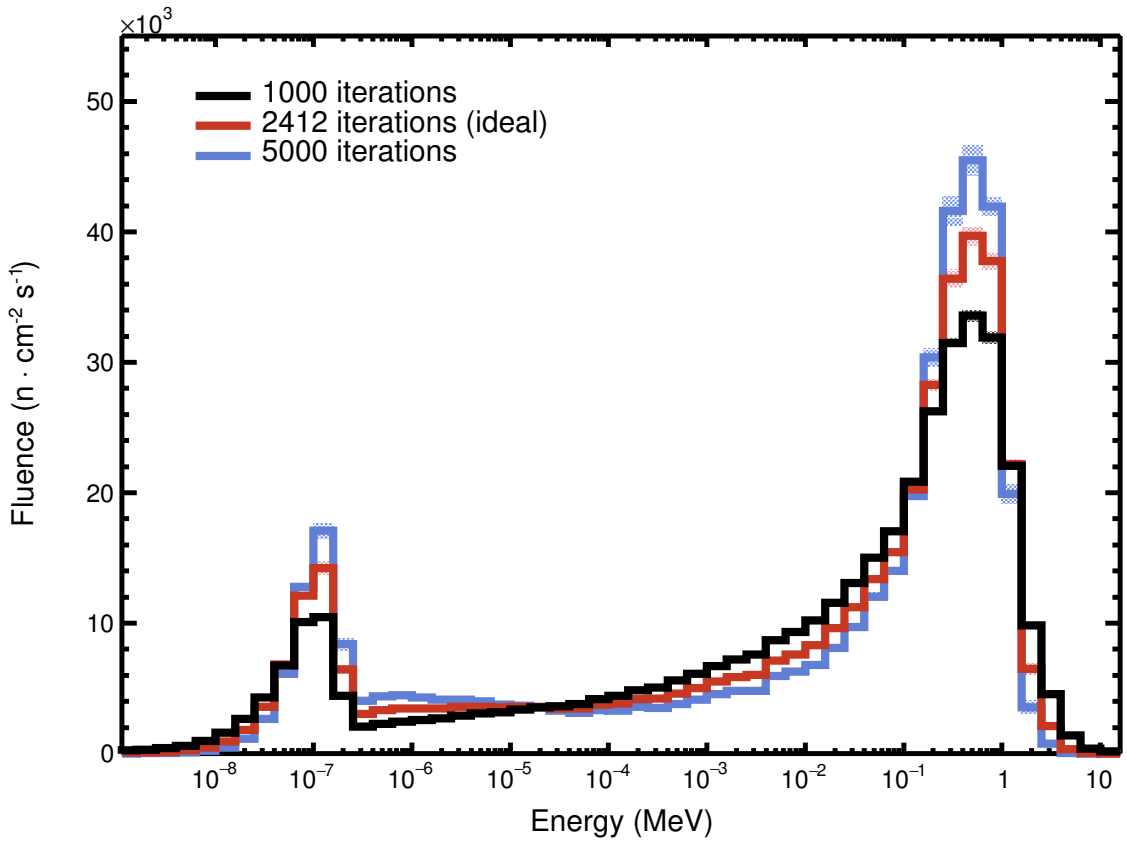

Figure 4.4 – Neutron fluence-rate spectrum determined using the conventional NNS for different MLEM iterations are plotted. The ideal spectrum (red) obtained for 2412 iterations and two other spectra for higher and lower iterations in blue and black respectively are shown in the graph.

4.3.1 Effect of the iteration number

The neutron fluence-rate spectrum determined using the passive NNS were obtained after unfolding the measured data for 2412 MLEM iterations as discussed before. This number of iterations was ideal for the conventional NNS data in order to obtain a sufficiently unfolded neutron fluence-

rate spectrum with a least amount of noise, as determined using the MLEM-STOP method. It is essential to understand the importance of the iteration number in obtaining the ideal spectrum after data unfolding.

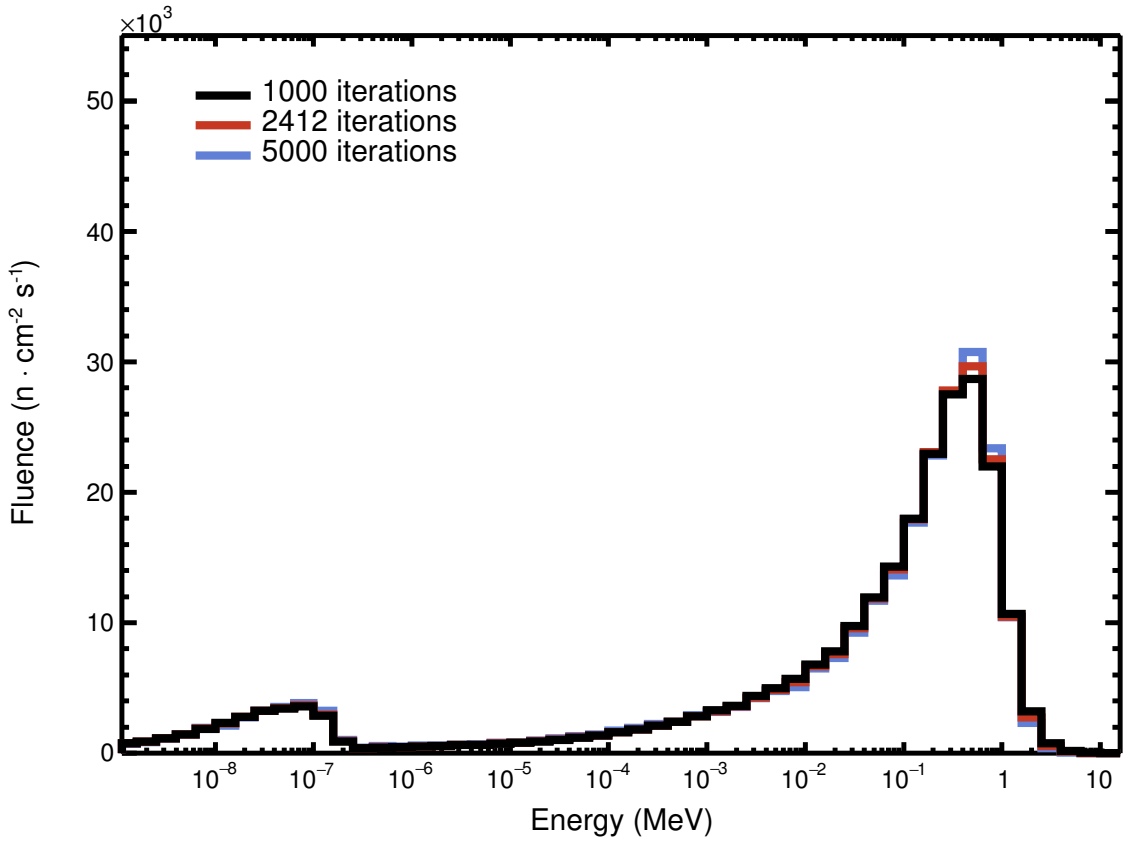

Figure 4.5 – Neutron fluence-rate spectrum determined using the passive NNS for different MLEM iterations are plotted. The spectra are not distinguishable because they overlay on each other.

Fig 4.4 shows how the neutron fluence-rate spectrum obtained using the conventional NNS varies with the MLEM iterations. The spectra obtained for iterations lower and higher than the ideal number that was determined using the MLEM-STOP method show significant differences between them. The spectrum obtained for 1000 iterations has lower thermal and fast peak, whereas

the spectrum obtained for 5000 iterations has higher peaks compared to the ideal spectrum. If the MLEM is let to unfold the data without terminating, the peak will continue growing, further unfolding the noise, as one would expect. Thus, it is crucial to stop the algorithm when the spectrum is sufficiently unfolded, and MLEM-STOP method takes care of this problem.

The effect of iteration number on the neutron fluence-rate spectrum obtained using the passive NNS is shown in Fig 4.5. Unlike the spectra obtained for the conventional NNS, the passive NNS spectra do not show significant variations. This is because the unfolding rates of the measured data are different for both passive NNS and conventional NNS.

4.3.2 Discussion

The development of a functioning passive NNS was successful and we were able to obtain the expected neutron fluence-rate spectrum using it. With the passive NNS, we could successfully but not exactly reproduce the shape of the active spectrum.

If we assume that the spectrum obtained using the passive NNS is the underlying true spectrum, then it may possible to attribute the difference between it and the spectrum obtained using the active NNS as an over response of the active NNS due to the conversion of charge measurement to count-rate using the calibration coefficient. However, because of the uncertainties in the neutron interaction cross-sections used in Geant4, especially for thermal energies, our confidence in the accuracy of the passive response functions is not absolute. Another important factor is the unfolding process itself. The passive NNS data were unfolded using the MLEM algorithm, and terminated when the iteration reached the same number (2412) as that used for the conventional NNS data via MLEM-STOP. Ideally, MLEM-STOP should be used to unfold the passive NNS data but it was not feasible because it was only possible to obtain a single set of measurements during the duration of this project. Because the passive NNS data converge/unfold at a different rate compared to the conventional NNS data, it is possible that we subjectively terminated MLEM before the passive

spectrum was sufficiently unfolded. Hence, they might agree better if both the data were unfolded using their own MLEM-STOP algorithms.

4.4 User's remarks on the passive NNS

The development of the passive NNS and its workflow were successful. The detector was able to measure the neutron fluence-rate spectrum in the radiotherapy bunker. Now that we have a streamlined set of procedures and a proof-of-principle result to use the passive system to obtain a neutron fluence spectrum, there is a potential to perform additional analyses with this system.

As with any detector, there are advantages and disadvantages with the passive NNS. The ability to perform spectral analysis accurately when the neutron fluence-rate is high is a key feature of the passive system. However, when the neutron fluence-rate is very low, the passive system with the gold foil may not be a good choice for fluence spectrum measurements. The induced activity will not be significant and consequently the measurement duration will be very long in such cases. Even in high neutron fluence-rate environments, the process of obtaining a neutron fluence spectrum can be time consuming compared to the active system which gives an immediate readout. In terms of operation, the passive detector is more economically demanding because of the gold foil used. The fact that the gold foils need to be replaced with new ones after a few irradiation is also something to be considered.

The passive NNS may not be a good candidate to perform the neutron fluence spectrum measurements on a daily basis. But it can be used in situations when the active system may need to be checked due to the high neutron fluence-rates.

4.5 Future works

Performing multiple measurements with the passive NNS to have enough data to perform MLEM-STOP unfolding would be the next logical task. We need to make sure that the discrepancy in neutron fluence-rate spectra is not due to any noise and random error. It is also essential to validate the response functions generated. Obtaining the fluence-rate spectrum from a neutron source, like Am-Be, whose spectrum is known may be one way to do it. Also, we can model the radiotherapy bunker and use Monte Carlo to simulate the neutron fluence-rate spectrum at the point of measurement and use it as the ground truth for spectral comparisons.

Chapter 5

Conclusions

In the research project described in this thesis, we developed and tested a passive NNS system that can be used in high neutron fluence-rate environments, such as in a radiotherapy bunker, to measure the neutron fluence spectrum. We modified the conventional NNS, which consists of a ^{3}He ionization chamber and moderator cylinders, by replacing the active ion chamber with passive activation foils, one foil per moderator configuration. Gold was chosen to be the foil material in our system because it complied with our foil requirements. Two cylindrical inserts were made to fill the gap where the ^{3}He chamber is normally housed inside the moderation system, and also to keep the gold foil at the geometric center of the system.

The response functions of the passive NNS were required in order to unfold the spectrum measurements obtained from the NNS. The detector was modelled in Geant4 and scored two parameters that were needed to determine the response functions of the passive NNS. Simulations were performed with 10^{7} neutrons, and with variance reduction techniques to obtain responses for 52 different energies and for all 8 moderator configurations.

A passive NNS system with a gold activation foil was successfully built and used in a high neutron fluence-rate environment in this work. The system was irradiated in a radiotherapy bunker

using a 15 MV photon beam and the gold foils became radioactive upon interacting with the photoneutrons generated as a byproduct of the beam.

The activated gold foils were analyzed using an HPGe gamma ray spectrometer to obtain the activities and MLEM algorithm unfolded these data to produce the neutron fluence-rate spectrum that corresponds to the point of measurement in the bunker.

The spectrum obtained using the conventional NNS was compared with that of the passive NNS to check the accuracy of conventional NNS's performance at high neutron fluence-rate environments.

The response functions generated for the passive NNS showed some significant features that were expected from the detector system. The neutron fluence-rate spectrum obtained was also in agreement with expectations; namely that two prominent peaks (the thermal and fast peaks) were observed. However, comparison of spectra from both the active and passive NNS showed some discrepancies at thermal and epithermal energies. Due to experimental limitations, application of the MLEM-STOP method to the passive data was not possible. The results seem promising but further studies are required to reliably draw a conclusion regarding the accuracy of the active NNS.

Appendix A

Derivation of specific saturation activity

Let us assume that the rate at which the gold foil is activated is G (activation rate). Activation rate is proportional to the neutron fluence rate. Also assume that the activation rate is constant, meaning that the neutron fluence rate from the linear accelerator is constant. This implies that the gold foil is activated at a steady rate.

If there are N radioactive nuclei in the gold foil, the rate at which they will decay can be written as λN, where λ is the decay constant of the ^{198}Au. The decay rate is also called as the activity of a radioactive sample [36].

In a real irradiation scenario, some of the radioactive ^{198}Au isotopes decay away during the time of irradiation itself. Therefore, the rate of change of N during the time of irradiation of the foil, when there is both activation and decay happening at the same time, is given by

$$\frac{dN}{dt} = G - \lambda N \tag{A.1}$$

Solving this differential equation for N = 0 at t = 0, we find that the number of radioactive ^{198}Au atoms present in the gold foil at any time t and it is given as

$$N(t) = \frac{G}{\lambda}(1 - e^{-\lambda t}) \tag{A.2}$$

Therefore, the activity of the sample at any time t is

$$\begin{aligned} A(t) &= \lambda N(t) \\ &= G\,(1 - e^{-\lambda t}) \end{aligned} \tag{A.3}$$

and the number of radioactive atoms is $N(t) = \frac{A(t)}{\lambda}$.

The activity builds up as the irradiation continues and when the activation rate becomes equal to the decay rate, it reaches a maximum called the saturation activity (A^{∞}). Mathematically, this can be show as

$$A^{\infty} = G \tag{A.4}$$

Now let us suppose the duration of irradiation was t_i. Then the activity of the gold foil after the completion of irradiation can be obtained from equations A.3 and A.4:

$$A(t_i) = A^{\infty}\,(1 - e^{-\lambda t}) \tag{A.5}$$

If the sampled is analyzed after a waiting time t_w and the activation analysis lasted a duration of measurement t_m, then the number of radioactive atoms in the gold foil before and after the

measurement would respectively be

$$N(t_i + t_w) = \frac{A(t_i + t_w)}{\lambda} = \frac{A^{\infty}}{\lambda}(1 - e^{-\lambda t_i})\, e^{-\lambda t_w} \tag{A.6}$$

,and

$$N(t_i + t_w + t_m) = \frac{A(t_i + t_w + t_m)}{\lambda} = \frac{A^{\infty}}{\lambda}\,(1 - e^{-\lambda t_i})\, e^{-\lambda t_w}\, e^{-\lambda t_m} \tag{A.7}$$

The number of decays that happened during the time of measurement is simply the difference of the number of atoms present in the foil before and after the measurement duration. Therefore, the number of decays expected during the gamma ray spectrometry (C_{exp}) can be obtained by subtracting equation A.7 from the equation A.6:

$$C_{exp} = \frac{A^{\infty}}{\lambda}(1 - e^{-\lambda t_i})\, e^{-\lambda t_w}\, (1 - e^{-\lambda t_m}) \tag{A.8}$$

However, the gamma counts measured with the spectrometer depends on the following factors:

1. Branching ratio (q) : it is the probability of emitting a gamma ray of interest during decay.

2. Detection efficiency (ε): The detection efficiency of the spectrometer for the gamma of a particular energy.

3. The background and dead time (B): The combined contribution of background signal and the loss of signal due to the dead-time of the detector.

Therefore, the counts measured with the spectrometer can be written as

$$\begin{aligned} C_{measured} &= (q\,\varepsilon\,C_{exp}) + B \\ &= q\,\varepsilon\,\frac{A^{\infty}}{\lambda}(1-e^{-\lambda t_i})\,e^{-\lambda t_w}\,(1-e^{-\lambda t_m}) + B \end{aligned} \tag{A.9}$$

Therefore,

$$A^{\infty} = \frac{\lambda\,(C_{measured}-B)\,e^{\lambda t_w}}{q\,\varepsilon\,(1-e^{-\lambda t_i})\,(1-e^{-\lambda t_m})} \tag{A.10}$$

The saturation activity per unit mass, also called the specific saturation activity, is therefore

$$A_s^{\infty} = \frac{\lambda\,(C_{measured}-B)\,e^{\lambda t_w}}{m\,q\,\varepsilon\,(1-e^{-\lambda t_i})\,(1-e^{-\lambda t_m})} \tag{A.11}$$

Bibliography

[1] Ahmedin Jemal, Freddie Bray, Melissa M Center, Jacques Ferlay, Elizabeth Ward, and David Forman. Global cancer statistics. *CA: a cancer journal for clinicians*, 61(2):69–90, 2011.

[2] Canadian Cancer Society, National Cancer Institute of Canada. Advisory Committee on Records, and Registries. *Canadian cancer statistics*. Canadian Cancer Society, 2018.

[3] Georges Al Makdessi. *Secondary neutrons around clinical electron and proton beams*. PhD thesis, McGill University Libraries, 2018.

[4] Robert Maglieri. *A Study of Photoneutron Spectra Around High-energy Medical Linear Accelerators Using Monte Carlo Simulations and Measurements*. PhD thesis, McGill University Libraries, 2015.

[5] Wouter Van Mechelen, Bert Aertgeerts, Karolien De Ceulaer, Bregje Thoonsen, Mieke Vermandere, Franca Warmenhoven, Eric Van Rijswijk, and Jan De Lepeleire. Defining the palliative care patient: a systematic review. *Palliative Medicine*, 27(3):197–208, 2013.

[6] Malin Dollinger and Ernest H Rosenbaum. *Everyone's Guide to Cancer Therapy;: How Cancer Is Diagnosed, Treated, and Managed Day to Day*. Andrews McMeel Publishing, 2002.

[7] Peter Nygren. What is cancer chemotherapy? *Acta Oncologica*, 40(2-3):166–174, 2001.

[8] Ervin B Podgoršak et al. *Radiation physics for medical physicists*. Springer, 2006.

[9] HR Vega-Carrillo, SA Martinez-Ovalle, AM Lallena, GA Mercado, and JL Benites-Rengifo. Neutron and photon spectra in linacs. *Applied Radiation and Isotopes*, 71:75–80, 2012.

[10] Tzinnia Gabriela Soto-Bernal, Antonio Baltazar-Raigosa, Diego Medina-Castro, and Hector Rene Vega-Carrillo. Neutron production during the interaction of monoenergetic electrons with a tungsten foil in the radiotherapeutic energy range. *Nuclear Instruments and Methods in Physics Research Section A: Accelerators, Spectrometers, Detectors and Associated Equipment*, 868:27–38, 2017.

[11] C Vega, L Perez, et al. Electro neutrons around a 12 mv linac. 2012.

[12] Jack Valentin. Relative biological effectiveness (rbe), quality factor (q), and radiation weighting factor (wr): Icrp publication 92. *Annals of the ICRP*, 33(4):1–121, 2003.

[13] Measurements. Scientific Committee 60. *Neutron Contamination from Medical Electron Accelerators: Recommendations of the National Council on Radiation Protection and Measurements*. Number 79. Ncrp, 1984.

[14] Mary PW Chin. Neutron contamination in a radiotherapy maze. *Master's thesis, University of Surrey*, 1999.

[15] Radiological Protection. Icrp publication 103. *Ann ICRP*, 37(2.4):2, 2007.

[16] RL Bramblett. Ewing. ri, bonner, tw. *Nucl. Instrum. Meth*, 9:1, 1960.

[17] DJ Thomas and AV Alevra. Bonner sphere spectrometers—a critical review. *Nuclear Instruments and Methods in Physics Research Section A: Accelerators, Spectrometers, Detectors and Associated Equipment*, 476(1-2):12–20, 2002.

[18] Sergio Morató, Belén Juste, Rafael Miró, Gumersindo Verdú, and Vicent Guardia. Evaluation of the response of a bonner sphere spectrometer with a 6lii detector using 3d meshed mcnp6. 1.1 models. *Radiation Physics and Chemistry*, 155:221–224, 2019.

[19] Hyeonseo Park and Jungho Kim. Recent activities of the neutron standardization at kriss. *Korea Research Institute of Standards and Science (KRISS), Korea*, 2015.

[20] J Dubeau, SS Hakmana Witharana, J Atanackovic, A Yonkeu, and JP Archambault. A neutron spectrometer using nested moderators. *Radiation protection dosimetry*, 150(2):217–222, 2011.

[21] Robert Maglieri, Angel Licea, Michael Evans, Jan Seuntjens, and John Kildea. Measuring neutron spectra in radiotherapy using the nested neutron spectrometer. *Medical physics*, 42(11):6162–6169, 2015.

[22] Logan Montgomery, Michael Evans, Liheng Liang, Robert Maglieri, and John Kildea. The effect of the flattening filter on photoneutron production at 10 mv in the varian truebeam linear accelerator. *Medical physics*, 45(10):4711–4719, 2018.

[23] TW Crane and MP Baker. Neutron detectors. *Passive Nondestructive Assay of Nuclear Materials*, pages 379–406, 1991.

[24] Judith F Briesmeister. Mcnpˆ< tm>-a general monte carlo n-particle transport code, version 4c. *LA-13709-M*, 2000.

[25] Roberto Bedogni. Neutron spectrometry with bonner spheres for area monitoring in particle accelerators. *Radiation protection dosimetry*, 146(4):383–394, 2011.

[26] K Amgarou, V Lacoste, H Muller, and F Fernández. Set-up of a passive bonner sphere system for neutron spectrometry at mixed fields with predominant photon component based on activation detector. *Radiation protection dosimetry*, 126(1-4):337–341, 2007.

[27] S Deepa, G Chaurasiya, YS Mayya, V Sathian, UV Phadnis, and DN Sharmab. Some studies in activation foils for measuring low-level induced activity for the neutron radiation protection.

[28] MB Chadwick, M Herman, P Obložinskỳ, Michael E Dunn, Y Danon, AC Kahler, Donald L Smith, B Pritychenko, Goran Arbanas, R Arcilla, et al. Endf/b-vii. 1 nuclear data for science and technology: cross sections, covariances, fission product yields and decay data. *Nuclear data sheets*, 112(12):2887–2996, 2011.

[29] Kalyanee Abging, Nirada Nanchamrud, Wanchai Dharmvanij, Wichian Ratanatongchai, and Somporn Chongkum. Neutron activation analysis of gold in soil. 2003.

[30] James S Welsh. Beta decay in science and medicine. *American journal of clinical oncology*, 30(4):437–439, 2007.

[31] Khalil Amgarou, VÉronique Lacoste, Alain Martin, Bruno Asselineau, and Laurent Donadille. Neutron spectrometry with a passive bonner sphere system around a medical linac and evaluation of the associated unfolding uncertainties. *IEEE Transactions on Nuclear Science*, 56(5):2885–2895, 2009.

[32] F Fernández, C Domingo, K Amgarou, J Castelo, T Bouassoule, MJ Garcia, and E Luguera. Neutron measurements in a varian 2100c linac facility using a bonner sphere system based on passive gold activation detectors. *Radiation protection dosimetry*, 126(1-4):361–365, 2007.

[33] Hidetsugu Ikegami, Kazusuke Sugiyama, Toshimitsu Yamazaki, and Mitsuo Sakai. Structure of platinum nuclei (i) new decay scheme of au196. *Nuclear Physics*, 41:130–158, 1963.

[34] D Win. Neutron activation analysis (naa). *AU J Technol*, 8(1):8–14, 2004.

[35] DJ Thomas, NP Hawkes, LN Jones, P Kolkowski, and NJ Roberts. Characterization and utilization of a bonner sphere set based on gold activation foils. *Radiation protection dosimetry*, 126(1-4):229–233, 2007.

[36] Glenn F Knoll. *Radiation detection and measurement*. John Wiley & Sons, 2010.

[37] GS Hubbard, EE Haller, and WL Hansen. Zone refining high-purity germanium. *IEEE Transactions on Nuclear Science*, 25(1):362–370, 1978.

[38] I. Kojouharov. Electrically cooled massive hpge detectors. Presented at the BgNS International conference nuclear power for people, Sozopol, Bulgaria, 2015.

[39] N S CEAN Sys. High purity germanium (hpge) detectors. Technical specifications, 2016.

[40] Michael F L'Annunziata. *Handbook of radioactivity analysis*. Academic press, 2012.

[41] Malvin H Kalos and Paula A Whitlock. *Monte carlo methods*. John Wiley & Sons, 2009.

[42] Pedro Andreo, David T Burns, Alan E Nahum, Jan Seuntjens, and Frank Herbert Attix. *Fundamentals of ionizing radiation dosimetry*. John Wiley & Sons, 2017.

[43] DWO Rogers and AF Bielajew. Monte carlo techniques of electron and photon transport for radiation dosimetry. *The dosimetry of ionizing radiation*, 3:427–539, 1990.

[44] Frank Herbert Attix. *Introduction to radiological physics and radiation dosimetry*. John Wiley & Sons, 2008.

[45] AB Chilton. A note on the fluence concept. *Health physics*, 34(6):715–716, 1978.

[46] AB Chilton. Further comments on an alternate definition of fluence. *Health physics*, 36(5):637–638, 1979.

[47] Lech Papiez and Jerry J Battista. Radiance and particle fluence. *Physics in Medicine & Biology*, 39(6):1053, 1994.

[48] K Amgarou and V Lacoste. Response matrix evaluations of a passive bonner sphere system used for neutron spectrometry at pulsed, intense and complex mixed fields. *Journal of Instrumentation*, 5(09):P09002, 2010.

[49] Forrest B Brown, RF Barrett, TE Booth, JS Bull, LJ Cox, RA Forster, TJ Goorley, RD Mosteller, SE Post, RE Prael, et al. Mcnp version 5. *Trans. Am. Nucl. Soc*, 87(273):02–3935, 2002.

[50] Francesc Salvat, José M Fernández-Varea, and Josep Sempau. Penelope-2008: A code system for monte carlo simulation of electron and photon transport. In *Workshop Proceedings*, volume 4, page 7, 2006.

[51] I Kawrakow and DWO Rogers. The egsnrc code system. *NRC Report PIRS-701, NRC, Ottawa*, 2000.

[52] GEANT Collaboration, S Agostinelli, et al. Geant4–a simulation toolkit. *Nucl. Instrum. Meth. A*, 506(25):0, 2003.

[53] Geant Collaboration. Introduction to geant4. 2010.

[54] Sea Agostinelli, John Allison, K al Amako, John Apostolakis, H Araujo, P Arce, M Asai, D Axen, S Banerjee, G 2 Barrand, et al. Geant4—a simulation toolkit. *Nuclear instruments and methods in physics research section A: Accelerators, Spectrometers, Detectors and Associated Equipment*, 506(3):250–303, 2003.

[55] Solomon Grigor'evich Mikhlin. *Integral equations: and their applications to certain problems in mechanics, mathematical physics and technology*, volume 4. Elsevier, 2014.

[56] Elena Resmerita, Heinz W Engl, and Alfredo N Iusem. The expectation-maximization algorithm for ill-posed integral equations: a convergence analysis. *Inverse Problems*, 23(6):2575, 2007.

[57] Lawrence A Shepp and Yehuda Vardi. Maximum likelihood reconstruction for emission tomography. *IEEE transactions on medical imaging*, 1(2):113–122, 1982.

[58] A P Dempster, N M Laird, and D B Rubin. Maximum likelihood from incomplete data via the em algorithm. *Journal of the Royal Statistical Society. Series B (Methodological)*, 39(1):1–38, 1977.

[59] F Ben Bouallègue, JF Crouzet, and D Mariano-Goulart. A heuristic statistical stopping rule for iterative reconstruction in emission tomography. *Annals of nuclear medicine*, 27(1):84–95, 2013.

[60] Logan Montgomery, Anthony Landry, Felix Mathew, and John Kildea. A novel mlem stopping criterion for unfolding neutron fluence spectra in radiation therapy. *Submitted to Nuclear Instruments and Methods in Physics Research Section A: Accelerators, Spectrometers, Detectors, and Associated Equipment*, 2019.

[61] Logan Montgomery, Anthony Landry, Felix Mathew, and John Kildea. Unfolding neutron fluence spectra in radiation therapy using a modified mlem-stop method. *The International Conference on the Use of Computers in Radiation Therapy and the International Conference on Monte Carlo Techniques for Medical Applications*, 2019.

[62] *Neutron Fluence Measurements*. Number 107 in Technical Reports Series. INTERNATIONAL ATOMIC ENERGY AGENCY, Vienna, 1970.

[63] Geant Collaboration. Geant4 user's guide for application developers. *Accessible from the GEANT4 web page [1] Version geant4*, 9, 2012.

[64] Emilio Mendoza, Daniel Cano-Ott, Tatsumi Koi, and Carlos Guerrero. New standard evaluated neutron cross section libraries for the geant4 code and first verification. *IEEE Transactions on Nuclear Science*, 61(4):2357–2364, 2014.

[65] M Herman, A Trkov, et al. Endf-6 formats manual. *National Nuclear Data Centre, BNL, Upton, New York*, 2005.

[66] G Kennedy and J St-Pierre. The neutron activation analysis laboratory at the ecole polytechnique de montreal. *Journal of radioanalytical and nuclear chemistry*, 180(2):347–351, 1994.